Inactivation of *Magel2* in a mouse model of Prader-Willi Syndrome alters autophagy in the hypothalamus and impairs muscle function

by

Ain Adilliah Kamaludin

A thesis submitted in partial fulfillment of the requirements for the degree of

Master of Science

in

Medical Sciences – Medical Genetics

University of Alberta

Abstract

Prader-Willi Syndrome (PWS) is a neurodevelopmental disorder causing severe neonatal hypotonia that persists until adulthood, reduced muscle mass, and hyperphagia leading to childhood-onset obesity. PWS is caused by inactivation of several genes located on chromosome 15q11-q13, including *MAGEL2.* MAGEL2 promotes endosomal protein trafficking through its interaction with TRIM27, an E3 RING ubiquitin ligase, and may also be important for delivering targeted proteins to lysosome to be degraded by a process known as autophagy. Mouse *Magel2* is predominantly expressed in the central nervous system, with higher expression in the hypothalamus, a key region in the brain that is responsible in regulating appetite and energy homeostasis. Loss of *Magel2* in mouse causes increased adiposity and reduced muscle mass, recapitulating abnormal phenotypes seen in people with PWS. Therefore, I hypothesize that *MAGEL2* plays a significant role in protein degradation by autophagy as well as regulation of body weight and muscle function. I determined that autophagy is dysregulated in specific hypothalamic neurons of *Magel2*-null mice. This was measured as a decrease in expression of p62, a protein that links targeted proteins for lysosomal degradation, and expression of ubiquitinated proteins in the neurons of mice lacking *Magel2*. Furthermore, *Magel2*-null mice have reduced muscle mass accompanied by changes in the muscle fiber size distribution, where a shift towards smaller fiber size was seen in gastrocnemius but a shift towards bigger fiber size was seen in soleus. No significant morphological changes were observed in *Magel2*-null muscles despite reduced muscle mass and changes in fiber size distribution. Loss of *Magel2* in muscle results in increased protein degradation associated with both an upregulation of *MuRF1*, a gene that regulates degradation of myofibrillar proteins, and increased p62 aggregates. Taken together, *Magel2* is required to maintain normal autophagic rate in hypothalamic neurons and plays important roles in regulating

muscle structure and function. Better understanding of the cellular function of *MAGEL2* in neuronal and muscle cells, and its connection with autophagy can be used to develop therapeutic treatments targeting neuronal autophagy, as well as muscle function and structure in children with PWS who lack *MAGEL2* expression.

Preface

Part of Chapter 2 and Chapter 3 in this thesis had been submitted for publication as Ain A. Kamaludin, Christa Smolarchuk, Jocelyn M. Bischof, Rachelle Eggert, Jun Ren, Joshua J. Lee, Toshifumi Yokota, Fred B. Berry, and Rachel Wevrick to the journal of *Human Molecular Genetics*. In chapter 2 of this thesis, Joshua Lee was responsible for differentiation of human fibroblasts to myotubes and RNA preparation from the myotubes. Dr. Wevrick was a corresponding author, while Dr. Yokota and Dr. Berry were the supervisory authors for the manuscript. The rest of Chapter 2 and Chapter 3 in this thesis are my original work.

The University of Alberta Animal Care and Use Committee approved all procedures involving animals in accordance with the guidelines of the Canadian Council on Animal Care.

Acknowledgements

First of all, I would like to thank Dr. Wevrick for giving me an opportunity to be one of her students and allowing me to learn so many techniques in her lab. My first year as a Master's student was so challenging with troubleshooting and negative results, but your encouragement and endless support motivated me to keep trying and not give up. You always made time to answer my questions and keep me on track. It was an amazing and memorable experience in my life to be part of your lab and I will be forever thankful for this experience.

I am also very grateful for getting a chance to join the Maternal and Child Health (MatCH) program and to do my rotation in Dr. Berry's and Dr. Yokota's lab. Thank you to the MatCH, the Canadian Institute of Health Research, and the Faculty of Medicine and Dentistry, University of Alberta for funding my stipend during graduate training.

Thank you to my committee members, Dr. Hughes and Dr. Goping for useful comments and suggestions to improve my project. Thank you to the members of the Wevrick laboratory, past and present, for a most enjoyable lab environment: Jocelyn for always helping me whenever I had issues with my experiments and arranging mice that I needed for my experiments; Chloe for helping me with mice work and being one of my best friends; Herman for proofreading my thesis; Vanessa for sharing so many of the ups and downs of graduate student life and for being my first best friend when I joined the department; and to all the others, which made the lab a great place to be in.

Finally, thank you to my friends and family. To Amirah and Siti, both of you always cheer me up, listen to my endless complaints and make me feel like I am with my own family. Without both of you, there is no way I could still be here in Edmonton and finish my degree. Thank you to my parents for their support when I decided to do a Master's and for their unconditional love. Finally to Cimi, my loving husband, for putting his faith in me to finish my studies and waiting patiently for me to come home to him.

Table of Contents

List of Tables

List of Figures

List of Abbreviations

AD – Alzheimer's disease

AgRP – Agouti-related peptide

AMPK – Adenosine monophosphate-activated protein kinase

AS – Angelman syndrome

Atg – Autophagy-related gene

AV – Autophagic vacuoles

Aβ – Amyloid-β

Baf A1 – Bafilomycin A1

BMD – Bone mineral density

BP – Breakpoint

CAG – Cytosine-adenine-guanine

CI-M6PR – Cation-independent mannose 6-phosphate receptor

CNS – Central nervous system

DNA – Deoxyribonucleic acid

E1 – Ubiquitin-activating enzyme

E2 – Ubiquitin-conjugating enzyme

EDL – Extensor digitorum longus

eIF3 – Eukaryotic translation initiation factor 3 subunit

ER – Endoplasmic reticulum

ESCRT – Endosomal sorting complex required for transport

FBS – Fetal bovine serum

FISH – Fluorescence in situ hybridization

GAA – Acid α-glucosidase

GFP – Green fluorescent protein

GSP – Gastrocnemius - soleus - plantaris

HD – Huntington's disease

HTT – Huntingtin

ID – Imprinting defect

LAMP-1 – Lysosome-associated membrane protein type 1

LAMP-2 – Lysosome-associated membrane protein type 2

LC3 – Microtubule-associated protein light chain 3

LCS –Long C-curve

MAFbx – Muscle Atrophy F-box

MAGE – Melanoma antigen

MEFs – Mouse embryonic fibroblasts

MG132 – N- (benzyloxycarbonyl)leucinylleucinylleucinal

MHC – Myosin heavy chains

MHD – MAGE homology domain

mTOR – Mammalian target of rapamycin

MuRF1– Muscle specific RING finger 1

MyoD1 – Myogenic differentiation 1

NGS – Normal goat serum

NPY – Neuro-peptide Y

NTS – Nucleus of tractus solitarus

ORF – Open reading frame

PBS – Phosphate buffer saline

PCR – Polymerase chain reaction

PD – Parkinson's disease

PE – Phosphotidylethanolamine

Pen-strep – Penicillin-streptomycin

PFA – Paraformaldehyde

PI3K – class III phosphatidylinositol 3 kinase

PI3P – Phosphotidylinositol 3-phosphate

POMC – Pro-opiomelanocortin

PVN – Paraventricular nucleus

PWS – Prader-Willi Syndrome

Q – Quadriceps

qRT-PCR – Quantitative reverse transcriptase-PCR

SCN – Suprachiasmatic nucleus

SM – Sternomastoid

SmN – Small nuclear ribonucleoprotein-associated protein N

snoRNAs – Small nucleolar RNA genes

SNURF – *SNRPN* upstream reading frame protein

SON – Supraoptic nuclei

SQSTM1 – Sequestosome-1

STAT3 – Signal transducer and activator of transcription 3

TA – Tibialis anterior

TBS – Tris-buffered saline

UPD – Uniparental disomy

α-MSH – α-melanocyte-stimulating hormone

β-ME – β-mercaptoethanol

1 Chapter 1: Introduction

1.1 Prader-Willi Syndrome

1.1.1 Prader-Willi Syndrome- Clinical characteristics

Prader-Willi Syndrome (PWS) is a complex genetic disorder characterized by hypotonia, hyperphagia leading to obesity, hypogonadism, short stature, and developmental delay (Holm *et al.*, 1993; Whittington *et al.*, 2004; Eiholzer *et al.*, 2006; Eldar-Geva *et al.*, 2010; Miller *et al.*, 2011). Prenatal-onset hypotonia manifests as reduced fetal movement, unusual fetal orientation and difficulty during delivery which can result in caesarian section or need for assisted delivery. Central hypotonia in infants is associated with poor sucking leading to difficulty feeding and lethargy, resulting in failure to thrive. Special feeding techniques such as nasogastric intubation or bottles with preemie nipples are mostly needed to assist feeding. Hypotonia usually improves over time but it persists until adulthood. Obesity is not seen in the first year of life. Obesity begins after onset of hyperphagia, which usually happens between the age of 1 and 4 years old. Food seeking behaviour is common including foraging for food, stealing of food or money to buy food and eating of inedible foods. Obesity and its complications (respiratory problems, sleep apnea, diabetes mellitus, thrombophlebitis, and chronic edema) are the major causes of morbidity and mortality in PWS.

Hypogonadism presents as genital hypoplasia, delayed pubertal development and infertility in both males and females with PWS. Genital hypoplasia is seen at birth and persists until adulthood. Smaller penis, cryptorchidism, and scrotal hypoplasia are often seen in males, while hypoplasia of the labia and clitoris are seen in females. Hypogonadism also results in delayed and incomplete pubertal development. Menarche may happen late by the age of 30, and amenorrhea or oligomenorrhea is also present in females. Males have poor growth of body and facial hair and rarely have voice changes. Short stature is mostly observed by the second decade of life due to lack of puberty growth spurt. PWS males have an average height of 155 cm and 148 cm for PWS females. Most individuals with PWS have mild intellectual disability (mean IQ: 60-70) together with delayed motor development and language milestones. A variety of less consistent features such as dysmorphic features, thick and viscous saliva, high pain threshold, skin picking, high threshold for vomiting, sleep disturbance, small hands and feet and hypopigmentation are also common in PWS.

The consensus clinical diagnostic criteria were revised and validated in 1993 by Holm and others, establishing with three different categories of clinical findings (major, minor and supportive). Major criteria are counted as one point, minor criteria are counted as half a point while supportive criteria had no point but increase certainty of other criteria (Holm *et al.*, 1993). Children aged 3 years and younger need 5 points for diagnosis, with 4 of these criteria coming from the major group and children over 3 years of age need 8 points for diagnosis, with 5 or more of these criteria coming from the major group. These clinical diagnostic criteria were published before molecular testing for PWS was available. The criteria were then revised in 2001 by Gunay-Aygun *et al*. after the genetic basis of PWS was discovered to assist diagnosis through deoxyribonucleic acid (DNA) testing. The newly revised criteria are suggested to prompt DNA testing for PWS: hypotonia and difficulty sucking in the first 2 years of age; global developmental delay with history of difficulty sucking and hypotonia in early childhood; global developmental delay, hyperphagia, with history of difficulty sucking and hypotonia in later childhood; or mild intellectual disability with behavioural problems, hypogonadism, and hyperphagia in adults (Gunay-Aygun *et al.*, 2001).

DNA methylation analysis is the most efficient way to begin a diagnosis as this is the only technique that will diagnose PWS in all three molecular classes (paternal deletion, uniparental disomy, imprinting defect Glenn *et al.*, 1996), which will be discussed later. However, DNA methylation analysis cannot be used to differentiate among molecular classes. After diagnosis of PWS is confirmed by DNA methylation analysis, another analysis can be done to determine the molecular classes. Fluorescence *in situ* hybridization (FISH) is used to identify deletion while DNA polymorphism analysis can be used to differentiate between uniparental disomy and imprinting defect (Smith *et al.*, 1993; Shaffer *et al.*, 2001; Hamzi *et al.*, 2010).

1.1.2 Research questions

The characteristics seen in PWS are associated with inactivation of several genes located on chromosome 15 (Ledbetter *et al.*, 1982; Robinson *et al.*, 1991). These genes include *SNURF-SNRPN*, *MKRN3*, *MAGEL2* and *NDN*, and a group of small nucleolar RNA genes (snoRNAs). In the Wevrick laboratory, we concentrate our studies on loss of *NDN* and *MAGEL2* function in contributing to PWS phenotypes. For my research project, I focused on the function of *MAGEL2* in the brain and muscle. The hypothalamus is a key region in the brain that regulates appetite and energy usage. Disruption in hypothalamic function is one of the causes of obesity in humans and mice. Loss of *MAGEL2* in the whole body including hypothalamus leads to alteration of body

weight, endocrine defects and metabolic disruption (Bischof *et al.*, 2007; Schaaf *et al.*, 2013), which strongly suggests a role for *MAGEL2* in the hypothalamus in maintaining appetite and energy metabolism. Unfortunately, little research on the cellular function of *MAGEL2* is available. In addition, autophagy disruption specifically in the hypothalamus alters body weight and metabolic function as seen in mice lacking autophagy-related genes (Kaushik *et al.*, 2011, 2012; Coupé *et al.*, 2012; Quan *et al.*, 2012). These phenotypes are consistent with phenotypes seen in mice lacking *Magel2* (Bischof *et al.*, 2007). Autophagy alteration due to loss of *MAGEL2* could be one of the causes of obesity in people with PWS and provides rationale for the study of the role of *MAGEL2* in regulating autophagic processes.

NDN and *MAGEL2* belong to the type II melanoma antigen (MAGE) gene group, and share a conserved region with 46% similarity at the amino acid level in this region (Chomez *et al.*, 2001; Doyle *et al.*, 2010). The Necdin protein is encoded by *NDN*, and is required for stimulating myoblast differentiation and for normal muscle growth (Deponti *et al.*, 2007; Bush and Wevrick, 2008). Lack of Necdin in fast and slow muscles impairs muscle development and muscle regeneration in mice. Children lacking *MAGEL2* function develop hypotonia and other musculoskeletal anomalies (Schaaf *et al.*, 2013). Since *MAGEL2* is highly related to *NDN*, it is possible that MAGEL2 might have a similar role as Necdin in regulating myogenesis and maintaining muscle growth. In addition to the role of autophagy in maintaining body composition, autophagy is also required for maintaining muscle mass. Autophagy inhibition in skeletal muscle results in muscle atrophy and reduced muscle strength (Masiero *et al.*, 2009). Hence, autophagy disruption in skeletal muscle may also contribute to muscle phenotypes seen in PWS.

1.1.3 Genetics of PWS

PWS is a contiguous gene disorder resulting from the loss of expression of several genes located on long arm of chromosome 15 (15q11-q13, Ledbetter *et al.*, 1982; Robinson *et al.*, 1991). Three major molecular mechanisms that lead to PWS are paternal deletion, maternal uniparental disomy (UPD) and imprinting defect (ID, Ledbetter *et al.*, 1982; Nicholls *et al.*, 1989; Robinson *et al.*, 1991; Glenn *et al.*, 1997). Paternal deletions account for the 65-75% of the cases that result from interstitial microdeletion of the paternally inherited chromosome 15q11-q13; 20-30% of cases are due to maternal UPD, in which both copies of chromosome 15 are inherited from the mother but neither from the father; and 1-3 % cases are caused by an imprinting defect (Woodage *et al.*, 1994; Cassidy *et al.*, 2012). Three different regions have been classified on chromosome

15q11-q13: non-imprinted, PWS, and Angelman syndrome (AS) regions (Figure *1.1*). Five protein-coding genes, including *SNURF-SNRPN*, *MKRN3*, *MAGEL2* and *NDN*, and snoRNAs located in PWS region are subjected to genomic imprinting which results in maternally silenced expression. However a recent publication by Schaaf et al. reported that loss of *MAGEL2* alone resulted in phenotypes resembling classic PWS or a Prader-Willi-Like syndrome, renamed to Schaaf-Yang Syndrome. (Schaaf *et al.*, 2013). The non-imprinted region is further divided into a proximal, non-imprinted region consisting of four biparentally expressed genes (*NIPA1*, *NIPA2*, *CYF1P1* and *TUBGCP5*) and a distal, non-imprinted region consisting of a group of three GABA receptor genes (*GABRB3, GABRA5* and *GABRG3*), *OCA2* and *HERC2*. Paternal deletions can be further divided into Type 1 deletion (between breakpoints BP1 and BP3) and Type 2 deletion (between breakpoints BP2 and BP3).

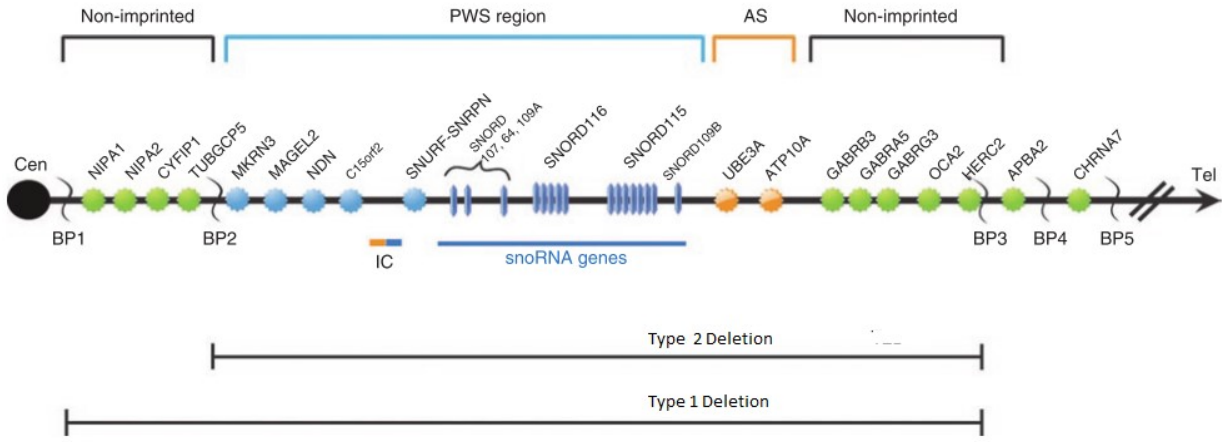

Figure 1.1 Overview of Prader-Willi/Angelman region on chromosome 15. Gene names in blue (PWS region) are paternally expressed and not expressed in PWS patients, whereas gene names in orange (AS region) are maternally expressed and not expressed in AS patients. Gene names in green (non-imprinted region) are expressed on both maternal and paternal chromosomes. Breakpoint (BP), imprinting centre (IC), centromere (Cen), telomere (Tel). Adapted from Cassidy *et al.*, 2012.

The *SNURF-SNRPN* locus is complex transcription unit encoding 148 exons, including *SNURF* (exon 1-4) which encodes *SNRPN* upstream reading frame protein (SNURF) and *SNRPN* (exon 4-10) which encodes small nuclear ribonucleoprotein-associated protein N (SmN), as well as a host of multiple small nucleolar RNA (snoRNAs) genes in its introns (Ozçelik *et al.*, 1992; Gray *et al.*, 1999; Cavaillé *et al.*, 2000; Runte *et al.*, 2001). SnoRNAs are a non-coding RNAs required for pre-rRNA splicing and are divided into two main classes, the C/D box and the H/ACA box snoRNAs (Cavaillé *et al.*, 2000; Scott and Ono, 2011). Out of 6 snoRNAs, SNORD115 (previously named *HBII-52*) is reported to modulate alternative splicing of serotonin receptor 2C mRNA by binding to exon Vb (Kishore and Stamm, 2006). *MKRN3* (also known as *ZNF127*), is a gene encoding makorin RING-finger protein 3. Loss of MKRN3 function alone causes central precocious puberty in humans (Jong *et al.*, 1999; Ap *et al.*, 2013).

NDN and *MAGEL2* encode proteins that belong to the MAGE protein family, and share a conserved region known as the MAGE homology domain (MHD) (Chomez *et al.*, 2001; Barker and Salehi, 2002). *NDN*, which encodes necdin protein, was found to be upregulated in mouse P19 embryonal carcinoma cells that were induced to differentiate into neurons when treated with retinoic acid (Maruyama *et al.*, 1991). Necdin is mainly expressed in post-mitotic neurons and plays an important role in neuronal differentiation (Kobayashi *et al.*, 2002; Takazaki *et al.*, 2002; Tennese *et al.*, 2008). Furthermore, necdin also acts as a growth suppressor by promoting cell-cycle exit (Hayashi *et al.*, 1995; Taniura *et al.*, 1998, 1999; Lee *et al.*, 2015). Necdin promotes myoblast differentiation (Deponti *et al.*, 2007; Bush and Wevrick, 2008; Pessina *et al.*, 2012), cell polarization (Bush and Wevrick, 2010) and inhibits programmed cell death (Hasegawa and Yoshikawa, 2008; Aebischer *et al.*, 2011; Huang *et al.*, 2013). The *MAGEL2* gene, encoding MAGEL2 protein, is expressed in adult brain tissues and in fetal brain, kidney and lung tissues (Lee *et al.*, 2000). The function of the MAGEL2 protein is not yet known, but recent findings by Doyle *et al*. and Hao *et al*. demonstrated that MAGEL2 binds to the E3 RING ubiquitin ligase, TRIM27 and promotes endosomal F-actin polymerization and retromer-mediated retrograde transport (Doyle *et al.*, 2010; Hao *et al.*, 2013). Many studies have been done on *Magel2*, a mouse ortholog of human *MAGEL2*, to better understand the function of MAGEL2 protein. Results from these studies will be described later.

1.1.4 Musculoskeletal manifestations and body composition in PWS

Common features of PWS are severe infantile hypotonia with difficulty feeding, developmental delay, and endocrine defects (Cassidy *et al.*, 2012). In addition, children with PWS are more likely to be born with hip dysplasia, club foot and vertebral anomalies compared to the normal population (Torrado *et al.*, 2013). People with PWS have abnormal body composition, with increased fat mass and reduced lean mass. This pattern starts in infancy and persists until adulthood (Reus *et al.*, 2011). Fat distribution is also unusual as the fat mass is accumulated in the limbs of people with PWS, but the reduction in lean mass is uniform throughout the body. This alteration of body composition in people with PWS suggests an abnormality in energy usage or partitioning. Infants and adults with PWS have significant reduction of energy expenditure due to decreased spontaneous physical activity, but also secondary to lower energy usage resulting from decreased lean mass, which is comprised mostly of muscle (Bekx *et al.*, 2003; Butler *et al.*, 2007). Children with PWS have reduced lower maximal muscle force and power with respect to body weight when jumping, and adults with PWS have 70% reduction of muscle strength in knee flexors, and difficulty in balancing (Capodaglio *et al.*, 2009, 2011; Edouard *et al.*, 2012). Physical therapy and growth hormone treatment improve body composition, muscle strength and endurance, and physical function in people with PWS (Eiholzer *et al.*, 2003, 2004; Wolfgram *et al.*, 2013).

Scoliosis is a common finding in children with PWS and the prevalence increases with age. Approximately 30% of PWS infants (ages 0-3), 29 % of children (ages 3-10), and 80% of adolescents were diagnosed with scoliosis (de Lind van Wijngaarden *et al.*, 2008). Two types of scoliosis were identified in PWS cases: long C-curve (LCS) type scoliosis and idiopathic scoliosis that is further classified according the Lenke classification system. Infants more commonly present with LCS, while adolescents only present with idiopathic scoliosis (type 5 and 6, Lenke system), and children present with both LCS and idiopathic scoliosis (de Lind van Wijngaarden *et al.*, 2008; Nakamura *et al.*, 2014b). Many children with severe scoliosis require brace treatment or surgical intervention to avoid life-threatening complications. Depending on age-, weight, or height-matched controls used for comparison, bone mineral density (BMD) has been reported to be normal or low in people with PWS (Edouard *et al.*, 2012; Nakamura *et al.*, 2014a). However, osteopenia/osteoporosis is common and begins in early childhood (Nakamura *et al.*, 2014a). The fracture risk is about 50% in children and 29% in adults with PWS (Butler *et al.*, 2002; Capodaglio *et al.*, 2011). Growth hormone treatment improved BMD in people with PWS but had no

significant effect on the prevalence or severity of scoliosis when compared to control group not treated with growth hormone (Carrel *et al.*, 2010; Nakamura *et al.*, 2014a).

1.1.5 *Magel2*-null mice- a mouse model of PWS

Magel2 is the mouse ortholog of *MAGEL2* and is located on mouse chromosome 7C region (Boccaccio *et al.*, 1999). The human and mouse Magel2 proteins are highly homologous and these putative proteins have 70% similarity. *Magel2* expression originates from the paternal allele but not from the maternal allele in the mouse brain. In the developing mouse, *Magel2* expression can be observed as early as embryonic day 9 (E9) in the central nervous system, including the neural tube, forebrain, midbrain, with a high level of expression in hypothalamus (Lee *et al.*, 2000; Kozlov *et al.*, 2007). *Magel2* expression was also detected in the dorsal root ganglia, neurons innervating the fore- and hindlimb buds, and trunk muscles. Outside of neuronal tissues, *Magel2* expression was restricted to the genital tubercle, midgut region, tongue and placenta. In the adult mouse brain, *Magel2* is highly expressed in neurons residing in the hypothalamus, including the suprachiasmatic nucleus (SCN), paraventricular nucleus (PVN) and supraoptic (SON) nuclei.

A *Magel2*-null mouse line was generated by replacing the open reading frame (ORF) of the *Magel2* gene with an in-frame LacZ knock-in expression cassette using a gene-targeting method (Kozlov *et al.*, 2007). Inactivation of mouse *Magel2* gene results in altered circadian rhythm output (Kozlov *et al.*, 2007; Devos *et al.*, 2011) and reduced fertility in both males and females. Decreased testosterone levels and mating frequency are observed in males while females show extended and irregular estrous cycles (Mercer and Wevrick, 2009). Magel2 is also required for proper food intake and leptin-mediated activation of pro-opiomelanocortin (POMC) neurons in hypothalamic arcuate nucleus (Bischof *et al.*, 2007; Kozlov *et al.*, 2007; Mercer *et al.*, 2013). *Magel2*-null mice are also characterized by delayed neonatal growth, excessive weight gain after weaning, reduced lean mass and increased adiposity with altered metabolism (Bischof *et al.*, 2007). These characteristics observed in *Magel2*-null mice resemble fundamental features of PWS phenotype, supporting the idea that the *Magel2*-null mouse is a promising mouse model to better understand MAGEL2 functions as they relate to PWS and Schaaf-Yang syndromes.

1.2 Autophagy in the brain

1.2.1 The autophagy process

Macroautophagy (hereafter autophagy) is a catabolic process that degrades cytosolic components such as proteins and organelles by delivering them to the lysosome. Autophagy is induced by various cellular stress signals, including the depletion of nutrients, hypoxia, endoplasmic reticulum (ER) stress, and specific types of protein aggregates (Nixon, 2013). Autophagy is a crucial process for maintaining cell survival and function. Inhibition of constitutive autophagy contributes to variety of neurodegenerative disorders including Alzheimer's disease, Parkinson's disease, and Hungtington's disease, which will be discussed below (Nixon, 2013; Kiriyama and Nochi, 2015). The major stages in autophagy involve formation of an isolation membrane (or phagophore), closure of the isolation membrane to form a double-membraned autophagosome, and fusion of the autophagosome with a lysosome to form an autolysosome (Figure 1.2).

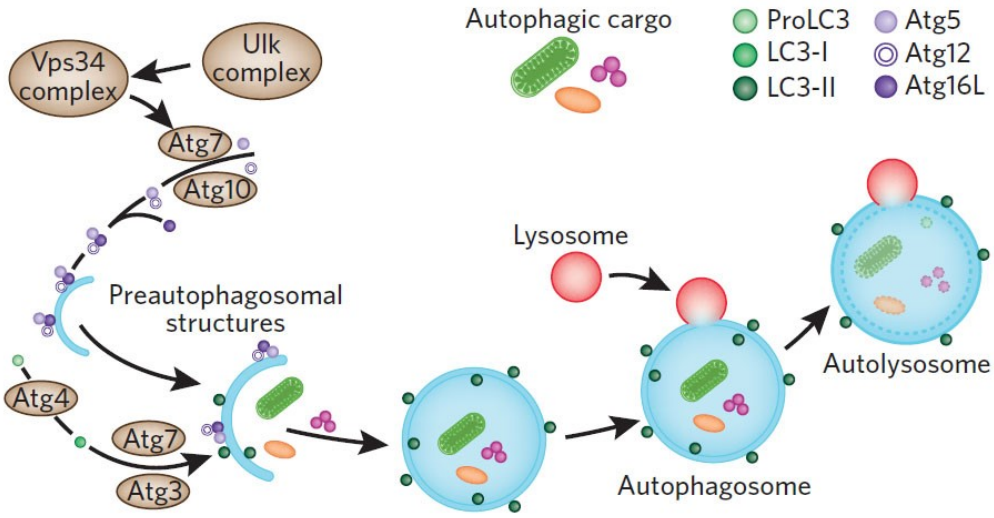

Figure 1.2 Schematic of autophagy. Autophagy initiation is regulated by phosphorylation status of the ULK complex after certain signals. The formation of the isolation membrane (phagophore, blue crescent) is mediated by the Vsp34 complex. Two conjugation steps occur: conjugation of Atg5-Atg12 by Atg 7 and Atg 10; and conjugation of LC3 with phosphotidylethanolamine (PE) by Atg4, Atg7 and Atg3. After that, the Atg12-Atg5-Atg16L complex and LC3-II are added to the elongating membrane. The membrane continues to elongate forming an autophagosome (blue circle). Fusion of an autophagosome and a lysosome leads to degradation of the autophagosomal contents by lysosomal hydrolases. Adapted from Fleming *et al.*, 2011.

Autophagy initiation is regulated by the phosphorylation status of one of the three hetero-oligomer complexes known as ULK complex (containing ULK1, ULK2, Atg13, FIP200, and autophagy-related gene (Atg) 101) (Mizushima, 2010). Mammalian target of rapamycin (mTOR) and adenosine monophosphate-activated protein kinase (AMPK) directly regulate ULK1 phosphorylation and control autophagy initiation (Shang and Wang, 2011; Laplante and Sabatini, 2013). Phosphorylation of ULK1 auto-activates it, then ULK1 phosphorylates the Vsp34-Vsp15-Beclin1-Bakor complex (Vsp34 complex), a component of the class III phosphatidylinositol 3 kinase (PI3K). This generates phosphotidylinositol 3-phosphate (PI3P), an important lipid substrate for autophagosomes. In the membrane elongation step, Atg5 and Atg12 are conjugated to each other in the presence of Atg7 and Atg10 enzymes, forming Atg12-Atg5-Atg16L complex on the isolation membrane, while Atg4, Atg7 and Atg3 covalently conjugated phosphotidylethanolamine (PE) to a cytosolic form of LC3 (LC3-I), adding conjugated LC3-II to the elongating membrane. An increase in the ratio of LC3-II to total LC3 protein indicates that autophagosome formation is increased. The membrane further elongates, encircling a part of the cytosol and forming an autophagosome. The last step for the autophagy process is fusion of the autophagosome with a lysosome generating autolysosome, and finally degradation of the autophagosomal contents by lysosomal hydrolases. Alternatively, the autophagosome can fuse with an early or late endosome to form an amphisome, which later fuses with lysosome for degradation.

Autophagy is generally recognized as a non-selective process, but new studies suggest that autophagy is a more selective process through the discovery of autophagic adaptor proteins that link targeted proteins to the phagophore membrane. LC3-II, a receptor protein on the phagophore membrane, interacts with adaptor proteins to induce their selective uptake and degradation of targeted proteins (Glick *et al.*, 2010; Nixon, 2013). The autophagic adaptors p62 (SQSTM1), and NBR1 recognize and facilitate the degradation of ubiquitylated protein by interacting with LC3 (Bjørkøy *et al.*, 2005; Kirkin *et al.*, 2009). In neurons, most autophagosomes are generated in axons and nerve terminals and greatly depend on retrograde transport to the cell body to complete autophagic degradation. During retrograde transport, most autophagosomes will fuse with late endosome forming amphisomes. The same proteins used for late endosome formation are required for amphisome formation, including Rab11 and the endosomal sorting complex required for transport (ESCRT) complexes (Rusten and Stenmark, 2009; Nixon, 2013).

1.2.2 Autophagy and neurodegeneration

Mutations in autophagy-related genes and the accumulation of autophagosomes in neurons are associated with several neurodegenerative diseases, such as Alzheimer's disease, Parkinson's disease and Huntington's disease (Nixon *et al.*, 2005; Yu *et al.*, 2005; Shibata *et al.*, 2006). Alzheimer's disease (AD) is characterized by dementia and morphological changes in the brain. Immuno-electron microscopy analyses shown accumulation of autophagosomes and late autophagic vacuoles (AV) within dystrophic neurites in an AD brain, suggesting an autophagy impairment in degrading aggregated and ubiquitylated proteins (Nixon *et al.*, 2005). The presence of amyloid plaques, consisting of accumulated amyloid-β (Aβ) peptides and the neurofibrillary protein with tau is another pathological feature in AD brain (Yu *et al.*, 2005; Kiriyama and Nochi, 2015). Deletion of presenilin 1, one of the components in the γ-secretase complex, plays an important role in V-ATPase maturation, causing a disruption in autolysosome acidification in AD neurons (Lee *et al.*, 2010). Taken together, autophagy impairment is associated with accumulation of AV and impairment of lysosomal acidification, leading to AD.

Parkinson's disease (PD) is the second most common neurodegenerative disease after Alzheimer's disease and is characterized by resting tremors, rigidity, bradykinesia and postural instability (Jankovic, 2008). The pathological feature of patients with PD is the accumulation of neuronal inclusions termed Lewy bodies, which are composed mostly of α-synuclein (Winslow *et al.*, 2010). Overexpression of α-synuclein caused by multiplication of the α-synuclein gene locus is a toxic mediator in sporadic PD. α-Synuclein overexpression also inhibits autophagy via Rab1A inhibition (Winslow *et al.*, 2010). Rab protein is a small GTPase, and various Rab proteins including Rab1A are required for autophagosome formation (Ao *et al.*, 2014). In addition, overexpression of α-synuclein and inhibition of Rab1A causes Atg9 mislocalization, which affects Atg9 function in autophagosome formation (Winslow *et al.*, 2010). Overexpression of RabA1 is able to rescue the loss of autophagosome caused by α-synuclein overexpression (Winslow *et al.*, 2010).

Huntington's disease (HD) is an autosomal dominant neurodegenerative disease characterized by motor dysfunction, cognitive impairment and psychiatric disturbances (Sumathipala *et al.*, 2013; Dayalu and Albin, 2015). HD is caused by expansion of cytosine-adenine-guanine (CAG) repeat at the 5' end of the huntingtin gene (HTT) and results in an extended polyglutamine (polyQ) stretch at the N terminus of huntingtin protein. Unaffected

individuals have 10 to 35 copies of the CAG repeats while people with HD have more than 36 copies of the CAG repeats (Shibata *et al.*, 2006). Huntingtin plays an important role in selective autophagy by interacting with ULK1 and p62 (Rui *et al.*, 2015). Huntingtin competes with mTOR for ULK1, releasing ULK complex from the inhibitory effect of mTORC1. Interaction of Huntingtin with p62 enhances recognition of cargo and binding to LC3. Deletion of the polyQ extension in Huntingtin has been shown to rescue neuronal autophagy and extends lifespan in HD mice (Zheng *et al.*, 2010), showing that conformational change of Huntingtin by expansion of polyQ can disrupt Huntingtin's role in selective autophagy.

1.2.3 Alteration of autophagy in neural cells

Among all cell types, neurons are particularly vulnerable to either increases or decreases in the autophagic clearance of autophagosome substrates. Neurons are post-mitotic cells and they cannot rely on cell division to prevent accumulation of damaged organelles and other cellular waste. Autophagy disruption in neurons results in accumulation of protein aggregates and neuronal degeneration. Studies looking at the importance of autophagy in central nervous system (CNS) have been increasing. A few studies have been reported using mouse models lacking Atg7 in the CNS or in POMC neurons, which regulate anorexigenic signals in the arcuate nucleus of hypothalamus. The first mouse model with conditional knockout of Atg7 was generated in 2005 (Komatsu *et al.*, 2005). They used Cre-loxP system to delete the Atg7 gene in the mice by breeding $Atg7^{F/F}$ mice with Zp3-transgenic mice, whose Cre recombinase expression is controlled by the ZP3 promoter in the oocyte. Atg-deficient mice have lower body weight when compared to control mice, have autophagosome puncta in the heart and die within 1 day after birth.

To better understand the role of autophagy especially in the CNS, another mouse model lacking Atg7 in the CNS was generated by breeding $Atg7^{F/F}$ mice with nestin-Cre transgenic mice (Komatsu *et al.*, 2006). Loss of Atg7 in the CNS severely affects neuronal survival and causes neuronal death in the cerebral and cerebellar cortices. Nestin-specific Atg7-deficient mice develop motor and behavioral deficits, have delayed growth development and reduced lifespan compared to control mice. Accumulation of ubiquitinated protein aggregates was also observed in various regions of the brain including cerebral cortex, cerebellum, hippocampus, hypothalamus and amygdala. Komatsu *et al.* concluded that autophagy is a key process to remove protein aggregates and plays a crucial role in neuronal survival, independent of the proteasome system.

In 2012, three research groups reported the importance of autophagy in regulating energy homeostasis by generating mice lacking Atg7, specifically in the hypothalamic POMC neurons (Coupé *et al.*, 2012; Kaushik *et al.*, 2012; Quan *et al.*, 2012). Coupé *et al.* demonstrated that autophagy occurs constitutively in POMC neurons under basal conditions by using transgenic mice that expressed GFP-tagged LC3. They bred $Atg7^{F/F}$ mice with POMC-Cre transgenic mice that express Cre recombinase under the control of POMC promoter (Coupé *et al.*, 2012). Deletion of Atg7 in POMC neurons resulted in increased body weight after weaning, higher fat mass, and other metabolic disturbances including insensitivity towards leptin and glucose intolerance in Atg7-deficient mice compared to control mice. In addition, age-dependent accumulation of ubiquitin and p62 in the arcuate nucleus and reduced neuronal projections of POMC neurons are also observed in POMC-specific Atg7-deficient mice. Results reported by Quan et al. and Kaushik et al. are consistent with these results. In addition, Quan *et al*. found that p62 colocalizes with ubiquitin in POMC neurons in Atg7-deficient mice. Moreover, POMC-specific Atg7-deficient mice have reduced energy expenditure, are more vulnerable to hyperglycemia after high-fat diet and have reduced signal transducer and activator of transcription 3 (STAT3) activation by leptin compared to control mice (Quan *et al.*, 2012). Kaushik et al. found a decrease in α-melanocyte-stimulating hormone (α-MSH), a cleavage product of POMC neurons and impaired lipolysis in Atg7-deficient mice compared to control mice (Kaushik *et al.*, 2012). Results from these studies show the importance of autophagy in POMC neurons in regulating neuronal survival, energy homeostasis, metabolic homeostasis and altered autophagy in the CNS leading to neurodegeneration in the mice.

Another mouse model with autophagy deficiency in the CNS was generated in 2006 by Hara *et al.* This group deleted Atg5, another autophagy-related gene, by breeding $Atg5^{F/F}$ mice with transgenic mice that express Cre recombinase under the control of nestin promoter (Hara *et al.*, 2006). Mice with Atg5 deletion in the CNS show characteristics similar to mice with Atg7 deletion in the CNS discussed previously. Mice with CNS-specific Atg5 deletion show progressive motor and behavioral deficits, delayed growth development and accumulation of ubiquitinated protein aggregates in the neurons in the thalamus, cerebral cortex, hippocampus, medulla and midbrain. In addition, they also observed degenerative changes in the neurons located in the cerebellum. Taken together, these results clearly suggest a critical role of autophagy in eliminating

unfavourable protein aggregates in the neuronal population and show that autophagy impairment in the CNS causes neurodegeneration in mice.

Disruption of autophagy by deletion of p62 impairs recognition of proteins targeted for degradation by the receptor protein, LC3. Deletion of p62 in the CNS surprisingly does not cause formation of inclusions in the neurons or neurodegeneration (Komatsu *et al.*, 2007a). Rather, deletion of p62 in Atg7-deficient liver and neurons inhibits the formation of ubiquitin-positive inclusions that usually accumulate in Atg7-deficient liver and neurons, and improves deleterious phenotypes seen in the liver due to Atg7 deletion, such as liver hypertrophy and high levels of serum aspartate aminotransferase, alanine aminotransferase and alkaline phosphatase. However, there is no improvement or worsening of neuronal phenotypes when p62 is deleted in Atg7-deficient neurons. These results suggest the pathological changes correlated with autophagic impairment are specific to the cell type. The deleterious phenotypes seen in Atg7-deficient neurons are not dependent on p62 while excess accumulation of p62 is a main cause of deleterious phenotypes seen in Atg7-deficient liver.

Interestingly, mice with p62 deletion become obese due to hyperphagia (Harada *et al.*, 2013). This finding suggests a possible role of p62 in modulating leptin signaling in the CNS. As expected, deletion of p62 in the CNS also leads to similar obesity seen in mice lacking p62 (Harada *et al.*, 2013). P62 is expressed in the arcuate nucleus, paraventricular nucleus and ventromedial hypothalamus, brain regions where leptin receptors are localized (Harada *et al.*, 2013). The expression of p62 is also observed in most POMC neurons, which regulate anorexigenic signals, and in some neuro-peptide Y (NPY) neurons, which regulate orexigenic signals in the arcuate nucleus of hypothalamus. Mice lacking p62 also have hyperlipidemia suggesting a disruption in leptin action in regulating food intake, but p62 deletion does not affect leptin-mediated depolarization of POMC neurons. In addition, mice lacking p62 show similar phosphorylation of STAT3 as control mice but have higher STAT3 accumulation in the nucleus of POMC neurons compared to WT mice. This study demonstrates the importance of p62 in regulating central energy balance and food intake.

1.3 Proteolysis in muscle

1.3.1 Fiber types in skeletal muscle

Other than in the brain, autophagy is also one of the important pathway that is required to maintain protein turnover in the skeletal muscles. Skeletal muscles are made of different fiber

types and consistently undergo dynamic processes of degeneration and regeneration. Analysis of single muscle fibers in the hindlimb muscles of rats identified four major myosin heavy chains (MHC) that include a slow type I fiber and three fast type (IIA, IID/IIX, IIB) containing type I, IIA, IID/X, and IIB myosin heavy chain isoforms respectively, and several intermediate hybrid fibers (MHCI + MHCIIA, MHCIIA + MHCIID/X, and MHCIID/X + MHCIIB) (Schiaffino and Reggiani, 1994). In C57BL6/J mice, the soleus muscles consist of type I, IIA and IID/X fibers with type IIA as the predominant fiber, unlike the rat soleus muscle, in which most of the fibers are type I (Augusto *et al.*, 2004). Tibialis anterior muscles predominantly have type IIB fibers with fewer type IID/X, IIA and I fibers. Gastrocnemius muscles contain all type of fibers, with type IIB as the most abundant fiber type followed by type IID/X, IIA and I fibers. Similar to the gastrocnemius, the extensor digitorum longus (EDL) muscles consist of all type of fibers with type IIB as the highest amount of fiber. The soleus muscle is classified as slow muscle while tibialis anterior, gastrocnemius and EDL are classified as fast muscles. Type I muscles are characterized as slow-twitch muscles that have high content of myoglobin and mitochondria (Neel *et al.*, 2013). Due to high content of myoglobin, type I muscles are red in colour, mainly perform oxidative metabolism and are invulnerable to fatigue. In contrast, type II muscles are characterized as fast-twitch muscles that have low content of myoglobin and mitochondria (Neel *et al.*, 2013). Type II muscles are white, mainly do glycolytic metabolism and are vulnerable to fatigue.

Skeletal muscles have various important roles in maintaining body posture, protecting and supporting internal organs, and producing voluntary and involuntary movements. Various conditions including increased body weight, decreased activity, physical and hormonal changes could impair muscle function. Genetically obese (ob/ob) mice that lack the adipose-derived hormone leptin have been used to determine morphological and biochemical changes in the skeletal muscle caused by obesity (Kemp *et al.*, 2009). The mean body mass of ob/ob mice is greater than the lean mice, whereas mean muscle mass is constantly lower than lean control mice. Measurement of total protein in sternomastoid (SM, fast muscle), EDL and soleus shows a significant low total protein in EDL and soleus but not in SM. Consistent with reduced mean muscle mass in ob/ob mice, the cross-sectional area of the muscle is smaller in SM (-29%), EDL (-24%) and soleus (-16%) in ob/ob mice compared to lean mice. In addition, smaller SM and EDL are associated with smaller fiber size but there is no difference in the mean fiber cross-sectional area for soleus. In terms of MHC composition, SM has more MHCIIA and MHCIID/X fibers and

fewer MHCIIB fibers; EDL has fewer MHCIIB fibers and more MHCIID/X; and soleus has more MHCI fibers and fewer MHCIIB. There is also a higher proportion of hybrid fibers in ob/ob muscle compared to lean muscle. Indeed obesity contributes to morphological and biochemical changes in ob/ob muscle with respect to size and fiber type composition.

1.3.2 Protein turnover in skeletal muscle

Protein turnover in skeletal muscle is regulated by two major signaling pathways, the autophagy-lysosome and ubiquitin-proteasome pathway (Sanchez *et al.*, 2014). The autophagy-lysosome system in skeletal muscle is similar to the autophagy system that has been discussed previously (section 1.2.1). In skeletal muscle, the ubiquitin-proteasome pathway is regulated by Akt/FOXO pathway and autophagy is also regulated by Akt/FOXO pathway in addition to regulation by mTOR/ULK1 pathway (Bonaldo and Sandri, 2013; Sanchez *et al.*, 2014). The mTORC1/ULK1 pathway only controls 10-12% of skeletal muscle autophagy while Akt/FOXO3 regulates 50% of skeletal muscle autophagy (Zhao *et al.*, 2007). Akt phosphorylates and inhibits FOXO3 in response to insulin or growth factor stimulation (Sanchez *et al.*, 2014). Activation of FOXO3 induces the expression of autophagy-related genes (*LC3, Gabarapl1, Vps34, ULK2, Atg12l, Atg4b, Bnip3* and *Beclin 1*), which are important for autophagy initiation and regulation (Mammucari *et al.*, 2007; Zhao *et al.*, 2007). Autophagy not only plays an important role in regulating neuronal survival and function, but is also crucial in maintaining muscle homeostasis. Disruption of autophagy in skeletal muscle causes atrophy due to reduced muscle mass, and this topic will be discussed later.

FOXO3 controls the autophagy and ubiquitin-proteasome pathways independently in skeletal muscle (Mammucari *et al.*, 2007). AMPK phosphorylates and activates FOXO3 under energy stress conditions such as nutrient deprivation and vigorous exercise (Figure *1.3*) (Sanchez *et al.*, 2014). Activation of FOXO3 induces the transcription of various E3 ubiquitin ligases including muscle Atrophy F-box (*MAFbx*)/*atrogin 1*, muscle specific RING finger 1 (*MuRF1*)/*Trim63* and *Trim32* (Bodine and Baehr, 2014; Sanchez *et al.*, 2014). Ubiquitin is covalently attached to targeted proteins through an enzymatic cascade that begins with addition of ubiquitin to ubiquitin-activating enzyme (E1) in an ATP-dependent manner, transferring ubiquitin to ubiquitin-conjugating enzyme (E2), and lastly to E3 ubiquitin ligase which then ubiquitinates a target protein (Bonaldo and Sandri, 2013). MAFbx regulates protein synthesis through degradation of the myogenic transcription factor MyoD, myogenin and the eukaryotic translation initiation

factor 3 subunit (eIF3) while MuRF1 and Trim32 control protein degradation by targeting myofibrillar proteins and components of thin filament respectively (Bodine and Baehr, 2014; Sanchez *et al.*, 2014). MAFbx and MuRF1 are transcriptionally upregulated in atrophic muscles, which make them suitable markers for muscle atrophy (Bodine *et al.*, 2001). Mice lacking MAFbx and MuRF1 are resistant to atrophy-inducing conditions, which suggests the roles of these two genes in regulating the atrophy process (Bodine *et al.*, 2001).

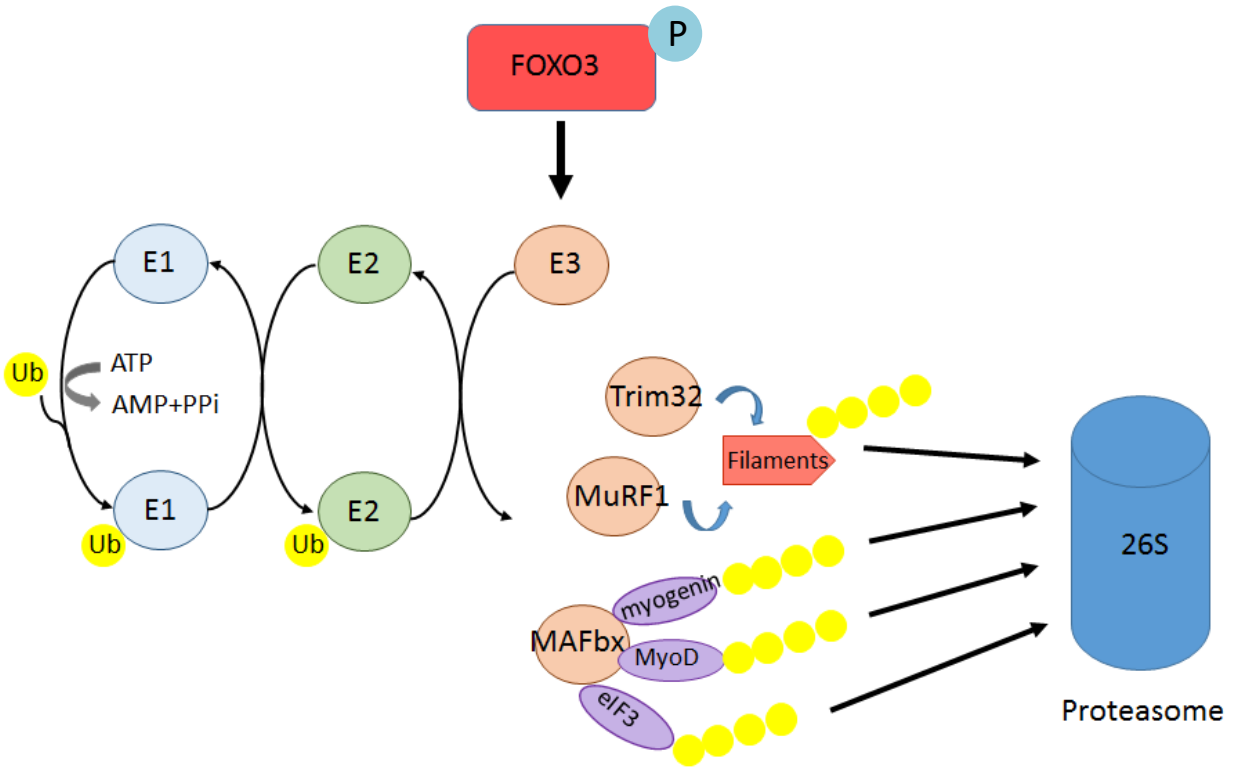

Figure 1.3 Schematic of ubiquitin-proteasome pathway. Ubiquitin is conjugated to proteins targeted to be degraded through ATP-dependent process, which requires E1-activating enzyme, E2-conjugating enzyme and E3 ubiquitin ligase. After the targeted proteins (MyoD, eIF3, myogenin in this schematic) are polyubiquitinated, they are attached to the proteasome for degradation. Activation of FOXO3 through phosphorylation increases the transcription of MAFbx, MuRF1 and Trim32. MAFbx regulates degradation of the myogenic transcription factor MyoD, myogenic and eIF3, while MuRF1 and Trim32 regulate degradation of several sarcomeric proteins and the components of thin filaments.

1.3.3 Autophagy maintain normal homeostasis of muscle mass

In transgenic mice expressing GFP-LC3, basal levels of autophagy in fast twitch muscle are similar to other tissues, and extremely low basal autophagy occurs in slow twitch muscle (Mizushima *et al.*, 2004). In fast twitch muscle, 24 hours of starvation causes increased autophagic rates while in slow twitch muscle, autophagic rates were slightly increased only after 48 hours starvation (Mizushima *et al.*, 2004). Starvation also induces protein degradation in fast muscle, both in the presence or the absence of insulin, but not in slow muscle (Frayn and Maycock, 1979). Both results suggest that different muscle fibers have specific regulation of protein degradation. Despite differential regulation of protein degradation in fast and slow muscles, the dynamic equilibrium between muscle autophagy and muscle generation is crucial in sustaining muscle mass and function.

Autophagy is important in regulating muscle mass and function as demonstrated in muscle-specific Atg7 knockout mice (Masiero *et al.*, 2009; Masiero and Sandri, 2010). Mice lacking Atg7 in the muscle show morphological changes including vacuolated and centrally nucleated myofibers, decrease in myofiber size by 40% and decreased absolute muscle force. Immunoblot and immunohistochemical analyses of muscle-specific Atg7-deficient mice showed accumulation of p62 and LC3 proteins, and lack of LC3 conjugation in protein lysates of adult fast and slow muscles, while p62 aggregates were observed in myofibers (Masiero *et al.*, 2009). Moreover, the expression of autophagy-related genes, *MAFbx*/*atrogin 1* and *MuRF1/Trim63* is upregulated in muscle-specific Atg7-deficient mice in the basal condition. In addition, autophagy inhibition induces muscle loss and degeneration in atrophy inducing conditions, such as denervation and fasting (Masiero *et al.*, 2009). Both of these conditions cause myofiber degeneration, but denervated muscles show severe atrophic phenotypes compared to fasted muscle. Atg7-deficient mice lose significantly more muscle mass, display more accumulation of inclusions and enlargement of p62 aggregates after denervation compared to after fasting. These results suggest a different role of autophagy in various atrophic conditions and show that autophagy is important for preserving muscle mass in both normal and pathological conditions.

Autophagy impairment is also observed in muscular dystrophy, which is a progressive degenerative muscle disease. Control and dystrophin-deficient (mdx) mice show similar basal levels of autophagy in both fast and slow muscles (Spitali *et al.*, 2013). Autophagy rates increase in slow muscle of control and mdx mice after 24 hours starvation, while autophagy induction is

only observed in fast muscle of control mice but not mdx mice after starvation. The expression of *MAFbx*, *Bnip3* and *MuRF1* is upregulated in control fast muscle after starvation but only *MuRF1* expression is upregulated in fast mdx muscle after starvation (Spitali *et al.*, 2013). This suggests that autophagy impairment in mdx fast muscle is mediated by FOXO3 transcription factor, and that autophagy is regulated differently in different muscles. Another animal model of muscular dystrophy, the collagen VI-deficient (Col6a1$^{-/-}$) mouse, has similar impairment in autophagy regulation (Grumati *et al.*, 2010). Collagen VI deficiency in muscle is correlated with mitochondrial dysfunction and muscle degeneration due to spontaneous apoptosis. Similar to mdx mice, autophagy is markedly impaired in fast Col6a1$^{-/-}$ muscle, while autophagy regulation is less compromised in slow Col6a1$^{-/-}$ muscle (Grumati *et al.*, 2010). Overall, autophagy is crucial in maintaining muscle mass and function while disruption or alteration in this process causes mild to severe muscle myopathy.

1.4 Rationale and hypothesis

Loss of function mutations in *MAGEL2* cause neonatal hypotonia, feeding difficulties, hyperphagia with excessive weight gain, hypogonadism, congenital hip dysplasia, club foot and proximal and distal joint contractures (Schaaf *et al.*, 2013). Phenotypes seen in people with lack of *MAGEL2* are consistent with phenotypes of *Magel2*-null mouse, which develop suckling problems, neonatal growth retardation, excessive weight gain after weaning, increased adiposity with hypothalamic dysfunction, and reduced fertility (Bischof *et al.*, 2007; Mercer and Wevrick, 2009; Schaller *et al.*, 2010; Mercer *et al.*, 2013). The consistency of phenotypes seen in people and mice caused by loss of *MAGEL2* function strongly suggests that *MAGEL2* must have a significant role in regulating body weight and the musculoskeletal development. However little is known about molecular function of *MAGEL2*.

MAGEL2 binds to an E3 RING ubiquitin ligase, TRIM27, and enhances the ubiquitin ligase activity of TRIM27 (Doyle *et al.*, 2010; Hao *et al.*, 2013). The MAGEL2-TRIM27 complex localizes to endosomes through interactions with retromer complex, which then promotes nucleation of F-actin via WASH complex and enhances endosomal protein recycling and trafficking. MAGEL2-TRIM27 activates WASH complex through K63-linked ubiquitination of WASH K220. Knockdown of MAGEL2-TRIM27 significantly disrupted retromer-mediated transport, showing that the MAGEL2-TRIM27 complex is essential for endosomal retrograde

transport. This suggests that MAGEL2 may also play a significant role in maintaining endosomal retrograde transport that involves protein recycling, trafficking and degradation.

The autophagy-lysosomal pathway is one of the major protein degradation pathways. Many emerging studies examined the role of autophagy in the CNS and muscle disorders (Komatsu *et al.*, 2005, 2006, 2007a; Hara *et al.*, 2006; Masiero *et al.*, 2009; Coupé *et al.*, 2012; Kaushik *et al.*, 2012; Quan *et al.*, 2012; Harada *et al.*, 2013). Disruption of autophagy specifically in the anorexigenic POMC neurons of mice results in growth retardation, increased body weight after weaning, increased adiposity, impaired hypothalamic function, insensitivity towards leptin and reduced axonal projections (Coupé *et al.*, 2012; Kaushik *et al.*, 2012; Quan *et al.*, 2012). These phenotypes are very similar to the phenotypes seen in mice lacking *Magel2*. Furthermore, inhibition of autophagy specifically in the muscle leads to decreased fiber size, reduced force generation, induced atrophy and development of myopathic features (Masiero *et al.*, 2009).

I hypothesize that obesity seen in PWS is caused by autophagy impairment due to the loss of *MAGEL2* in the hypothalamus, specifically in the POMC neurons that are critical for regulating body homeostasis. Further, I hypothesize that the loss of *MAGEL2* in skeletal muscle disrupts various pathways during musculoskeletal development including autophagy, which leads to infantile hypotonia and other musculoskeletal abnormalities in PWS. My objectives for this thesis project were to determine whether loss of *Magel2* disrupts autophagy in the hypothalamus and to assess the role of *Magel2* in musculoskeletal development.

2 Chapter 2: Materials and Methods

2.1 Animals and cell cultures

2.1.1 Mouse strains

Procedures involving animal were approved by the University of Alberta Animal Care and Use Committee in accordance with Canadian Council on Animal Care Guidelines. Wild-type and *Magel2*-null mice were generated as described (see Section 1.1.4) and are available from the Jackson Laboratory (C57BL/6-*Magel2*^{tm1Stw}/J, #009062, Bischof *et al.*, 2007). Mice were weaned between 3 to 4 weeks of age and then group-housed with standard food (PicoLab Mouse Diet 20, LabDiet) and water *ad libitum*, and sustained under 12:12 light:dark cycle. Genotyping was done by PCR of ear notch biopsies or by β-galactosidase activity in unused brain tissue (by Jocelyn Bischof in our laboratory, Gérard *et al.*, 1999; Bischof *et al.*, 2007). In experiments involving brain tissue, Magel2$^{+/-}$ carrier males were crossed with homozygous POMC^{EGFP} reporter mice (Jackson Laboratories stock #009593) to generate Magel2: POMC^{EGFP} experimental offspring, which lack *Magel2* expression but express GFP in POMC cells. Control littermates express both *Magel2* and the GFP reporter gene (Pravdivyi *et al.*, 2015).

2.1.2 Generation of primary mouse embryonic fibroblasts

Timed breeding was set up and the date was recorded when a vaginal plug was visible. Embryos were then collected at day 16 of gestation to generate primary mouse embryonic fibroblasts (MEFs) as follows. The pregnant mouse was euthanized and dissected to remove uterine horn containing the embryos. The uterine wall was torn open and the embryos were taken out. The umbilical sac, head and liver were carefully separated and removed. The umbilical sac and liver were discarded while the head was placed in a micro-centrifuge tube containing Lac Z staining solution for genotyping. All blood clots in body cavity were removed using forceps and the remainder of the embryo was rinsed with sterile phosphate buffer saline (PBS). After the head and liver were removed, each embryo was minced with a razor blade and transferred to a 15 ml conical flask containing 2 ml of 0.25% trypsin/1 mM EDTA, incubated for 15 min at 37ºC and the tissues were then vigorously pipetted to suspend cells. 500 µL of cell suspension was transferred to a T25 flask containing 4 ml fresh Dulbecco's modified Eagle's medium (DMEM) with 20% fetal bovine serum (FBS) and 1% penicillin-streptomycin (pen-strep), for a total of 4 flasks per embryo. Cells were passaged at least 2 times before they were used for subsequent experiments.

2.1.3 Culturing of primary hypothalamic neurons

Hypothalamic tissues were taken from pups at postnatal day 5 to generate primary hypothalamic neuron cultures. Pups were sacrificed by removing the head and placing it in a new petri dish covered with Hank's solution (containing 1.5% HEPES and 0.3% pen-strep, Gibco by Life Technologies) to remove excess blood. The brain was removed from the head and both hemispheres were gently separated using forceps. The hypothalamus was collected from both hemispheres and was placed into a new Falcon tube. The following steps were performed in a tissue culture hood. Hypothalamic tissues were rinsed 3 times with 4 – 5 ml of Hank's solution and about 0.5 – 1 ml was kept at the end of the rinse. Tissues were incubated at 37 ºC with 0.5 ml trypsin for 15 min. Tissues were rinsed with Hank's as above, followed by incubation with 0.5 ml FBS for 30 seconds and rinse with Hank's.

In order to remove non-neuronal cells, 1 ml of Day 1 culture medium (neurobasal medium from Gibco by Life Technologies containing 1.5% HEPES, 1.5 % sodium pyruvate, 10 % FBS, 0.3 % L-glutamine, and 0.3 % pen-strep) was added and tissues were dissociated by pipetting up and down without making bubbles, and then transferred to a new petri dish with 2 ml culture medium and incubated in culture medium for 30 min at room temperature. After 30 min, the culture medium was collected from petri dish and was centrifuged for 5 min at 2700 x g. The supernatant was aspirated and the cell pellet was re-suspended in 2 ml of Day 1 culture medium and split into 2 wells of 6 well plate containing coverslip coated with poly-L-Lysine (Sigma-Aldrich). Half of the culture medium was changed on every odd day with Day 3 culture medium (neurobasal medium containing 1.5% HEPES, 1.5 % Sodium pyruvate, 10 % FBS, and 0.3 % pen-strep) for day 3 and with Day 5 culture medium (neurobasal medium containing 1.5% HEPES, 1.5 % Sodium pyruvate, 1 % N2 supplement, 0.3 % pen-strep, and 10 µM AraC (Sigma-Aldrich) for day 5 and onwards.

2.1.4 Differentiation of human fibroblasts into myotubes

Human control fibroblasts were cultured in growth medium containing DMEM/F-12 1:1 (Invitrogen, San Diego, CA, USA), 20% or 10% FBS, and 1% pen-strep. In T25 flask, 70-80% confluent fibroblasts were transduced with retroviruses expressing MyoD and GFP construct. After 24 hours incubation, growth medium was replaced and incubation was continued until numerous GFP^+ cells are observed. The GFP^+ cells were collected, FACS-sorted and seeded into growth medium. After 24 hours incubation with growth medium, the medium was replaced with

differentiation medium containing DMEM with 0.1% gentamycin, and ITS Liquid Media Supplement (Sigma-Aldrich, St. Louis, MO, USA), and cultured for 18 days (Saito *et al.*, 2010). The process of converting MyoD-expressing fibroblasts to myotubes and the preparation of RNA from these cultures was done by Joshua Lee and Yusuke Echigoya in Dr. Toshifumi Yokota's laboratory (University of Alberta).

2.2 Protein analysis

2.2.1 Cell treatments

Primary MEFs were seeded at a density of 3.0 x 10^5 cells per well of a 6 well plate. The next day, primary MEFs were treated with Bafilomycin A1 (Baf A1) for 4 hours as follows: control (media containing 0.1% DMSO), serum-starved with Baf A1 (serum-free media containing 100 nM Baf A1), or Baf A1 (media containing 100 nM Baf A1). Cells were collected for protein analysis (see Section 2.2.2). Additional primary MEFs were treated with MG132 as follows: control (media containing 0.1% DMSO), serum-starved with MG132 (serum-free media containing 25 μM MG132), MG132 (media containing 25 μM MG132), or MG132 with Baf A1 (media containing 25 μM MG132 and 100 nM Baf A1). Primary MEFs were incubated with these MG132 treatments for 6 hours before the cells were collected for protein analysis.

2.2.2 Crude protein preparation

Tissues were collected, transferred into a micro-centrifuge tube, and snap frozen in liquid nitrogen. The tissues were ground using a disposable plastic pestle and resuspended in 2X modified sample buffer (20% glycerol, 4% SDS, 0.13 M Tris, pH 7.8) with Complete Mini protease inhibitor (Roche). In the case of cultured cells, the cells were rinsed with PBS and suspended with trypsin. Suspended cells were then centrifuged at 300 x g for 5 min and rinsed with PBS. The rinsed cells were centrifuged as before and re-suspended in 2X modified sample buffer. The tissues/cells were sonicated on ice (3 times for 5 seconds with 5 seconds pause), incubated (65ºC for 5 min) then centrifuged (10 min at 20800 x g). The supernatant was transferred to new micro-centrifuge tube and stored at -80ºC. For immunoblots, protein was thawed then 2 μL/100 μL of 2% β-mercaptoethanol (β-ME) and 1 μL/100 μL of saturated bromophenol blue were added, then boiled for 5 min in a boiling water bath and stored at -20ºC.

2.2.3 Immunoblotting

A range of 10 µg to 15 µg of protein depending on the experiment was electrophoresed on a 12 % polyacrylamide gel (to detect p62 and ubiquitin) or 14 % polyacrylamide gel (to detect LC3). Resolved proteins were then transferred to a PVDF membrane and blocked at room temperature for 1 hour with 5 % non-fat dry milk in Tris-buffered saline with 0.1 % Tween-20 (TBST). The blot was incubated overnight at 4ºC with rabbit anti-SQSTM1/p62 (Abcam ab91526, 1:1000 dilution), rabbit anti-LC3B (Cell Signaling #2775, 1:1000 dilution), rabbit anti-Ub (DAKO Z0458, 1:300 dilution) diluted in blocking buffer, or for 2 hours at room temperature with mouse anti-β actin (Sigma A3854,1:50000 dilution). Blots were washed in TBST, then incubated in anti-rabbit or anti-mouse HRP secondary antibody (Amersham NA934V and Amersham NA931V, 1:1000 dilution), diluted in blocking buffer, for 1 hour at room temperature. Chemiluminescent HRP substrate (Millipore) was used to develop the blot and image was captured with Kodak Image Station 4000mm. Immunoblot analysis was performed using Kodak Image Station Software and protein quantities were calculated as the ratio of band intensity from the protein of interest to band intensity from β-actin.

2.3 Brain analysis

2.3.1 Brain fixation and sectioning

Wild-type and *Magel2*-null mice expressing GFP in POMC neurons were euthanized and perfused intracardially with 4% paraformaldehyde (PFA) in PBS. The brains were removed, post-fixed with 4% PFA overnight at 4ºC and cryoprotected in PBS containing 20% sucrose until the brain sank. These brains were embedded with cryomatrix (OCT) (Thermo Scientific) and frozen on dry ice. Cryosections (30 µm) were collected in coronal plane through the entire arcuate nucleus.

2.3.2 Immunohistochemistry

Brain sections from mice expressing GFP in POMC neurons were blocked with PBS containing 10% normal goat serum (NGS) and 0.3% Triton X-100 for 1 hour at room temperature and incubated with primary antibody (Rabbit anti-SQSTM1/p62, 1:1000 or rabbit anti-Ub, 1:300) diluted in PBS containing 1% NGS and 0.3% Triton X-100 overnight at 4ºC. Goat anti-rabbit Alexa Fluor 546 secondary antibody (Thermo Fisher Scientific A11035, 1:1000 dilution) was diluted in PBS containing 1% NGS and sections were then rinsed with PBST and then incubated

in secondary antibody for 1 hour at room temperature. ProLong Gold antifade reagent with DAPI (Life Technologies) was used to mount the sections. Sections were imaged using a Zeiss LSM 510 confocal microscope and analysis was done using Image J (NIH). GraphPad Prism version 5 was used for statistical analysis. Experiment was done on a few brain sections from single biological sample, which are >90 μm apart to ensure that neurons in the first brain section are not the same neurons as in the second brain section.

2.4 Muscle analysis and histology

2.4.1 Muscle dissection and sectioning

Wild-type (unfasted and fasted for 24 hours) and *Magel2*-null (unfasted) mice were euthanized then the skin was removed from both hind legs. Three muscle groups (gastrocnemius –soleus-plantaris (GSP), quadriceps (Q), and tibialis anterior (TA) were dissected from both hind legs, weighed, then embedded with cryomatrix (OCT). The blocks were immersed in cold isopentane and frozen on liquid nitrogen. Cryosections (12 μm) were collected in transverse plane through the entire muscle tissue.

2.4.2 Muscle immunohistochemistry

Muscle sections were blocked with PBS containing 10% NGS and 0.3% Triton X-100 for 1 hour at room temperature. Anti-SQSTM1/p62 (1:1000 dilution) and anti-dystrophin (Abcam ab15277, 1:400) were diluted in PBS containing 1% NGS and 0.3% Triton X-100. Sections were incubated in primary antibody overnight at 4ºC and incubated in secondary antibody for 1 hour at room temperature. Goat anti-rabbit Alexa Fluor 546 secondary antibody (Thermo Fisher Scientific A11035, 1:1000 dilution) was diluted in PBS containing 1% NGS. ProLong Gold antifade reagent with DAPI was used to mount the sections. Sections were imaged using a Wave FX spinning disk confocal microscope and analysis was done using Image J (NIH). GraphPad Prism version 5 was used for statistical analysis.

2.4.3 Hematoxylin and eosin staining

Transverse sections (12 μm) were collected from GSP and TA muscle. Sections were incubated in hematoxylin solution for 10 min (Electron Microscopy Sciences, 26043-05). Sections were then rinsed with running tap water for 15 min and incubated with 1% aqueous eosin Y solution (Electron Microscopy Sciences, 26762-1A) for 10 min. After the incubation, sections were dipped for 1 second in 70% ethanol followed by 90% ethanol, and 2 times 30 seconds in

100% ethanol. Sections were then incubated in xylene 2 times for 5 min each and mounted with VectaMount permanent mounting medium (Vector Laboratories). Images were taken using a Nikon Eclipse TE2000-U inverted research microscope.

2.5 RNA analysis

2.5.1 RNA extraction

Trizol reagent (1 ml per 50-100 mg of tissue, Ambion by Life Technologies) was added to the muscle tissues and a disposable plastic pestle was used to grind the tissues. Homogenized tissues were incubated at room temperature for 5 min and chloroform (0.2 ml per 1 ml of Trizol used) was added after incubation. The tissues (sample) were mixed thoroughly and incubated at room temperature for 2 to 3 min. After the incubation, the sample was spun down at 12000 x g for 15 min at 4ºC. The aqueous phase was separated from the phenol-chloroform phase and the interphase, and transferred to a fresh tube. Isopropanol (0.5 ml per 1 ml of Trizol used) was added to the aqueous phase, mixed well and incubated at room temperature for 10 min. The sample was centrifuged at 12000 x g for 10 min at 4ºC to obtain RNA pellet and supernatant was removed from the tube after centrifugation. The RNA pellet was washed with 75% RNAse-free ethanol (1 ml per 1 ml of Trizol used) and was centrifuged at 7500 x g for 5 min at 4ºC. The ethanol supernatant was removed after centrifugation. The tube containing the RNA pellet was air-dried on bench, then the pellet was dissolved in 20-30 µl of Rnase-free water. Dissolved RNA was incubated for 10 min at 55-60ºC and store at -80 ºC. The RNA concentration of each sample was measured using GE NanoVue Plus spectrophotometer before use.

2.5.2 Real-time RT-PCR

cDNA was generated using 1 µg of RNA in a 20 µL reaction volume and the Superscript II First-Strand Synthesis System (Invitrogen). Only 10% of the cDNA generated from the first-strand reaction was used for polymerase chain reaction (PCR). The PCR reaction was performed with *Taq* DNA polymerase. A list of reverse transcriptase-PCR (RT-PCR) used for the experiment is shown in **Table 1**. All quantitative reverse transcriptase-PCR (qRT-PCR) reactions were performed in a 20 µL volume and 2x QuantiTect SYBR Green PCR Master Mix (Qiagen) was used. All reactions were performed on a 7900HT Fast Real-Time PCR System. A list of qRT-PCR primers used for the experiments is shown in **Table 2**. The qRT-PCR experiment was replicated 2-3 times for *MAFbx* and *MuRF1* expression and was performed once for mouse *Magel2*

expression. Cycling conditions for qRT-PCR were 15 min at 95ºC, 40 cycles of 94ºC for 15 seconds, 57ºC for 30 seconds, and 72ºC for 30 seconds. Additional cycles were done for melting temperature analysis to confirm purity. Expression levels were measured using $2^{-\Delta\Delta Ct}$ method (Livak and Schmittgen, 2001).

Table 1 List of forward and reverse primers used for RT-PCR

Genes	Forward primer (5' – 3')	Reverse primer (5' – 3')
Human *MAGEL2*	AAAAGACCGCATGATCTTTGCT	GACCTCCCAGTCACTCAGATTTAG
Human *GAPDH*	TCCCTGAGCTGAACGGGAAG	GGAGGAGTGGGTGTCGCTGT

Table 2 List of forward and reverse primers used for qRT-PCR

Genes	Forward primer (5’ – 3’)	Reverse primer (5’ – 3’)
Mouse *MuRF1*	GTGTGAGGTGCCTACTTGCTC	GCTCAGTCTTCTGTCCTTGGA
Mouse *MAFbx*	CACATTCTCTCCTGGAAGGGC′	TTGATAAAGTCTTGAGGGGAA
Mouse *Tbp*	CCTTGTACCCTTCACCAATGAC	ACAGCCAAGATTCACGGTAGA
Mouse *Magel2*	GGCTGCACTCTACGAGAACC	GGCATTTGCGTCCTTGTATT
Human *MAGEL2*	CCTGGGCTCCGCTAAATCATT	TCATGCGGTCTTTTGAAGGGG
Human *SDHA*	GAAGCATAAGAACATCGGAACTG	CTGATTTTCCCACAACCTTCTTGC

2.6 Statistical analyses

Means and standard deviations were calculated for normally distributed continuous data and comparisons between groups were done by Student's unpaired two-sided t-test (Graphpad, La Jolla, California) or by two-way ANOVA with post-hoc testing as appropriate. A Mann-Whitney test was used for continuous data that was not normally distributed and Fisher exact test was used for categorical data. P values are considered statistically significant when $P<0.05$ and are indicated when statistical test results were $P<0.1$.

3 Chapter 3: Results

3.1 Autophagy occurs in the hypothalamus and in primary MEFs of *Magel2*-null mice under basal conditions

Autophagy is an important cellular degradation and recycling process, which occurs constitutively in neuronal cells including hypothalamic POMC neurons (Mizushima *et al.*, 2004; Boland *et al.*, 2008; Coupé *et al.*, 2012). Disruption of autophagy in neural cells has been reported to cause neurodegenerative diseases in human and in mice (Ravikumar *et al.*, 2004; Hara *et al.*, 2006; Komatsu *et al.*, 2006; Boland *et al.*, 2008). MAGEL2, which belongs to the melanoma antigen (MAGE) protein family is highly expressed in the hypothalamus and is known to interact with and bind to E3 RING ubiquitin ligases, promoting protein trafficking and recycling (Lee, S. Walker, C L. Wevrick, 2003; Kozlov *et al.*, 2007; Doyle *et al.*, 2010; Hao *et al.*, 2013). Inactivation or knockdown of MAGEL2, one of the critical components in the MAGEL2-TRIM27 complex markedly disrupts nucleation of endosomal F-actin and retromer-mediated transport including retrograde transport of cation-independent mannose 6-phosphate receptor (CI-M6PR) to the trans-golgi network and integrin α5 to the plasma membrane (Hao *et al.*, 2013).

To determine whether autophagy occurs in the brain of *Magel2*-null mice, I performed immunoblots on protein lysates collected from the hypothalamus. Various autophagy markers were used to examine autophagy including LC3, SQSTM1/p62 and ubiquitin. LC3 has been effectively and widely used to assess autophagosome formation *in vivo* (Mizushima *et al*. 2004). I detected similar expression of conjugated LC3-II protein in the hypothalamus of *Magel2*-null mice compared to wild type (WT) control mice, indicating that autophagosome formation and autophagy occur in both genotypes (Figure *3.1*A-B). I also determined the levels of p62 protein and ubiquitinated protein in the hypothalamus of *Magel2*-null mice and WT mice. I found that the levels of p62 and ubiquitinated protein in the hypothalamus of *Magel2*-null mice are similar to WT mice (Figure *3.1*A-C). These results demonstrate that normal autophagy occurs in the hypothalamus of both WT and *Magel2*-null mice.

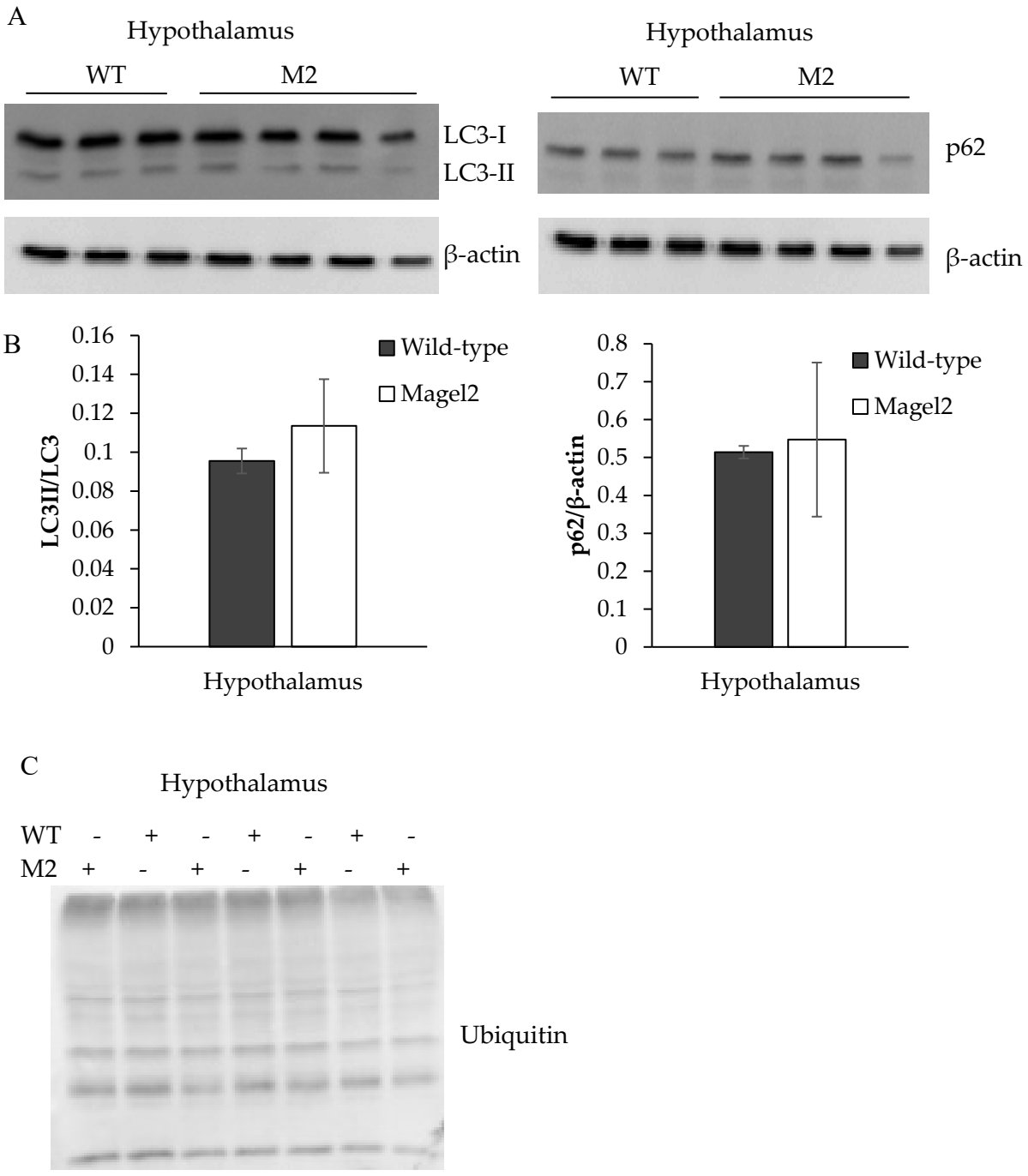

Figure 3.1 Measurement of autophagy markers; LC3, p62 and ubiquitin in hypothalamus. A) LC3 and p62 expression in the hypothalamus of WT and *Magel2*-null (M2) mice. A similar ratio of LC3-II to total LC3 and similar abundance of p62 were found in hypothalamus from both genotypes. B) Quantification of LC3-II to total LC3 (LC3-I + LC3-II) and p62 immublots in A. C) Immunoblot against ubiquitin showing similar amounts of ubiquitylated proteins in WT and M2 hypothalamus. WT N=3, Magel2 N=4. LC3-I=16 kDa, LC3-II=14 kDa.

I also assessed the levels of autophagy markers in primary MEFs. I detected similar levels of conjugated LC3-II, p62 and ubiquitinated protein in WT and *Magel2*-null primary MEFs (Figure *3.2*A-C). I then examined the levels of autophagy in primary MEFs when autophagy is induced, together with late-phase autophagy inhibition. I induced autophagy by removing serum from culture media and adding Baf A1, a late-phase autophagy inhibitor (Bjørkøy *et al.*, 2005). Animal serum is a vital component in culture medium as it provides fundamental factors including growth, hormonal, stabilizing and detoxifying factors for the cells to survive *in vitro* (Brunner *et al.*, 2010). Serum starvation stresses the cell and eventually leads to autophagy induction (Steiger-Barraissoul and Rami, 2009). While serum starvation increases autophagy, Baf A1 blocks incorporation of the autophagosome with the lysosome hence preventing the degradation of autophagic vacuoles (Yamamoto *et al.*, 1998). This condition will lead to increased conjugated LC3-II and p62 expression in the cells.

I observed a significant effect of genotype (higher expression in *Magel2* primary MEFs compared to WT primary MEFs, P=0.0004, two-way ANOVA) on conjugated LC3-II expression and on p62 expression (higher expression in *Magel2* primary MEFs compared to WT primary MEFs, P<0.0001, two-way ANOVA) (Figure *3.3*). However there was no significant difference between genotypes for conjugated LC3-II and p62 expression in either treatment in post-hoc analysis. The results illustrate that autophagy occurs in both genotypes regardless of autophagy induction and inhibition, while basal autophagy is maintained.

In addition to increased expression of autophagy markers when autophagy is inhibited, I examined the expression of conjugated LC3-II and p62 proteins when proteasome degradation is blocked (Figure *3.4* and Figure *3.5*). The proteasome inhibitor MG132 has been used to block protein degradation by the 26S proteasome in primary MEFs (Goldberg, 2012). In three different treatments (serum starvation+MG132, MG132 only and MG132+Baf A1), there was no significant effect of genotype and treatment on conjugated LC3-II expression (Figure *3.4*). For p62 expression, there was a significant effect of genotype (higher expression *Magel2* primary MEFs compared to WT primary MEFs, P<0.0001, two-way ANOVA) but no significant effect of treatment (Figure *3.5*). However, the difference in conjugated LC3-II and p62 expression between genotypes was not statistically significant in all treatments. In summary, I observed that autophagy occurs at basal condition in both WT and *Magel2*-null hypothalamus and primary MEFs.

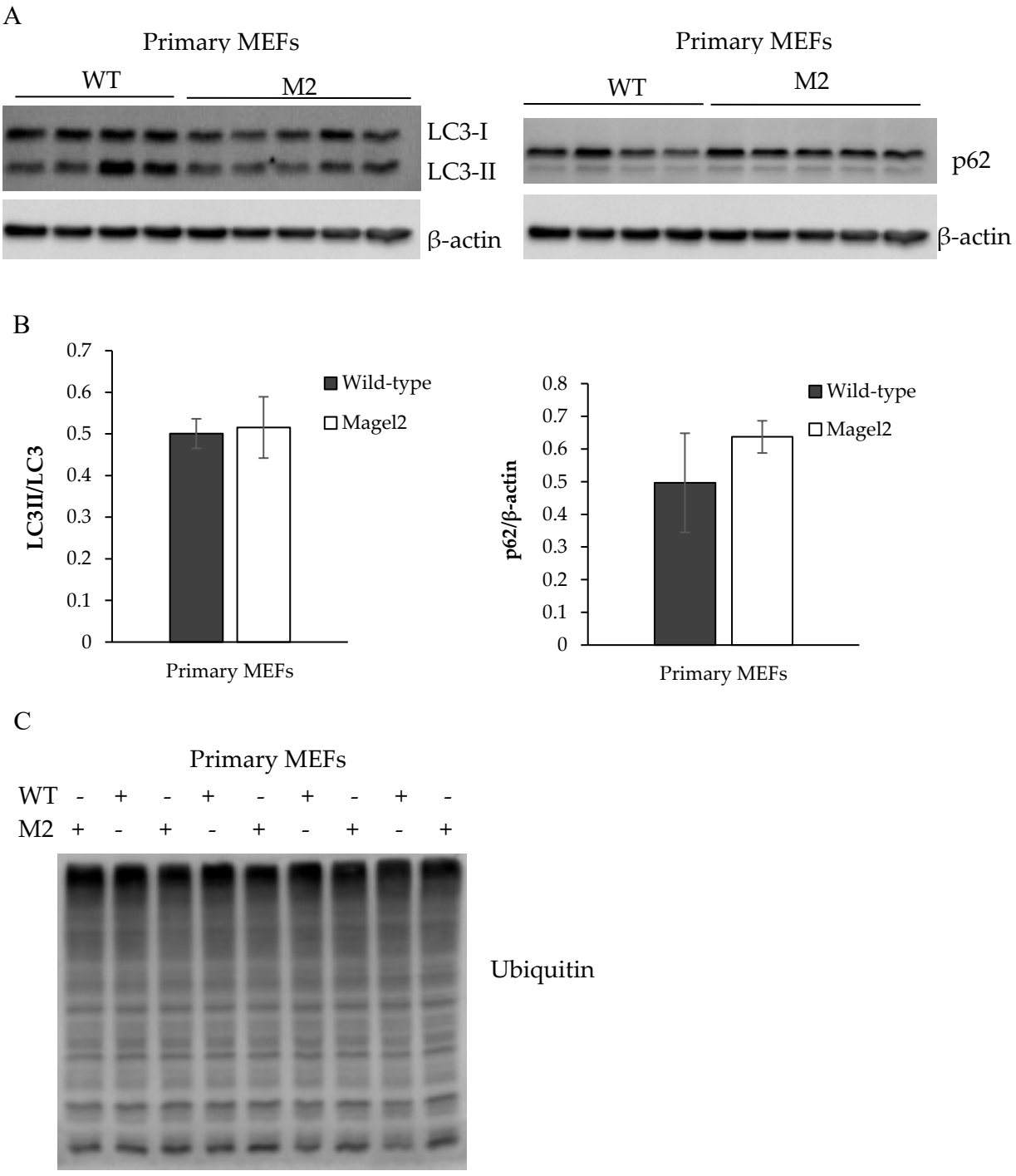

Figure 3.2 Measurement of autophagy markers; LC3, p62 and ubiquitin in primary MEFs. A) LC3 and p62 expression in WT and *Magel2*-null (M2) primary MEFs. A similar ratio of LC3-II to total LC3 and similar abundance of p62 were found in primary MEFs from both genotypes. B) Quantification of LC3-II to total LC3 (LC3-I + LC3-II) and p62 immunoblots in A. C) Immunoblot against ubiquitin showing similar amounts of ubiquitylated proteins in WT and M2 primary MEFs. WT N=4, Magel2 N=5. LC3-I=16 kDa, LC3-II=14 kDa.

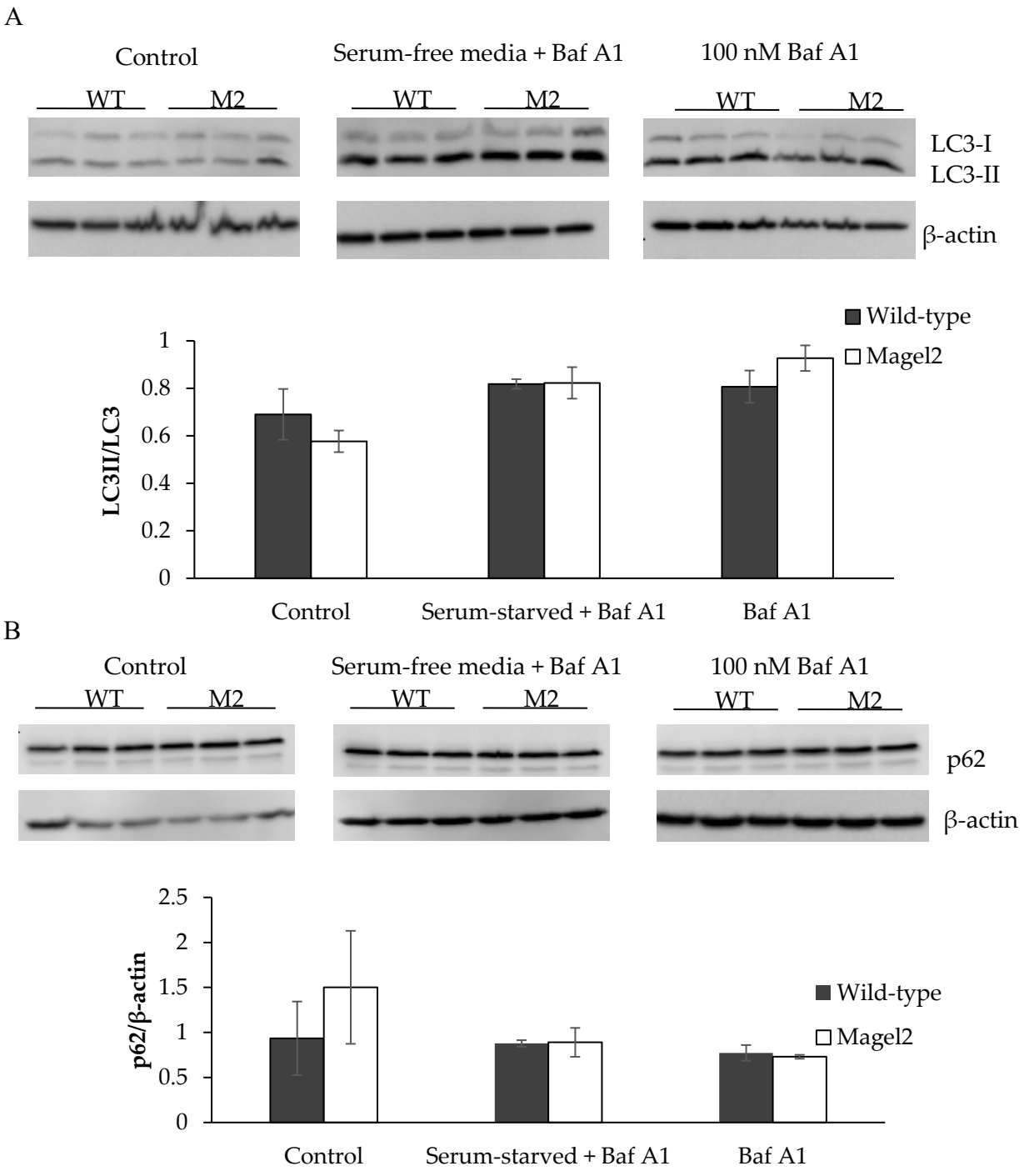

Figure 3.3 Autophagy levels in primary MEFs treated with 100 nM Baf A1 for 4 hours. A) LC3 expression in WT and *Magel2*-null (M2) primary MEFs with 3 different treatments (above) and quantification of LC3-II to total LC3 (LC3-I + LC3-II) in the above blot (below). B) p62 expression in WT and M2 primary MEFs with 3 different treatments (above) and quantification of p62 band in the above blot (below). WT N=3, Magel2 N=3. LC3-I=16 kDa, LC3-II=14 kDa.

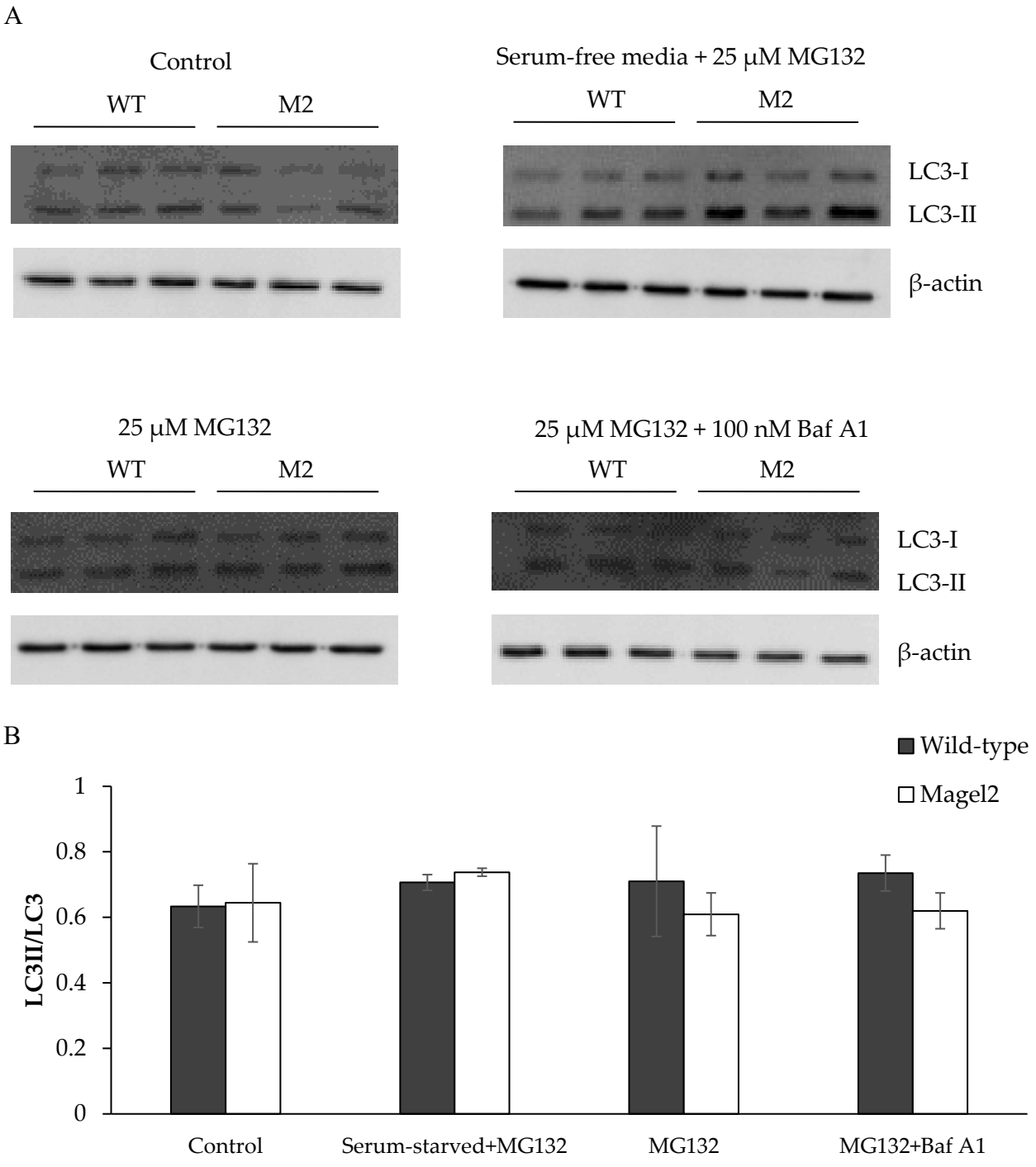

Figure 3.4 LC3 expression in primary MEFs treated with 25 μM MG132 and 100 nM Baf A1 for 6 hours. A) Blots showing LC3 expression in WT and *Magel2*-null (M2) primary MEFs treated with 4 different treatments. B) Quantification of LC3-II to total LC3 (LC3-I + LC3-II) in A. WT N=3, Magel2 N=3. LC3-I=16 kDa, LC3-II=14 kDa.

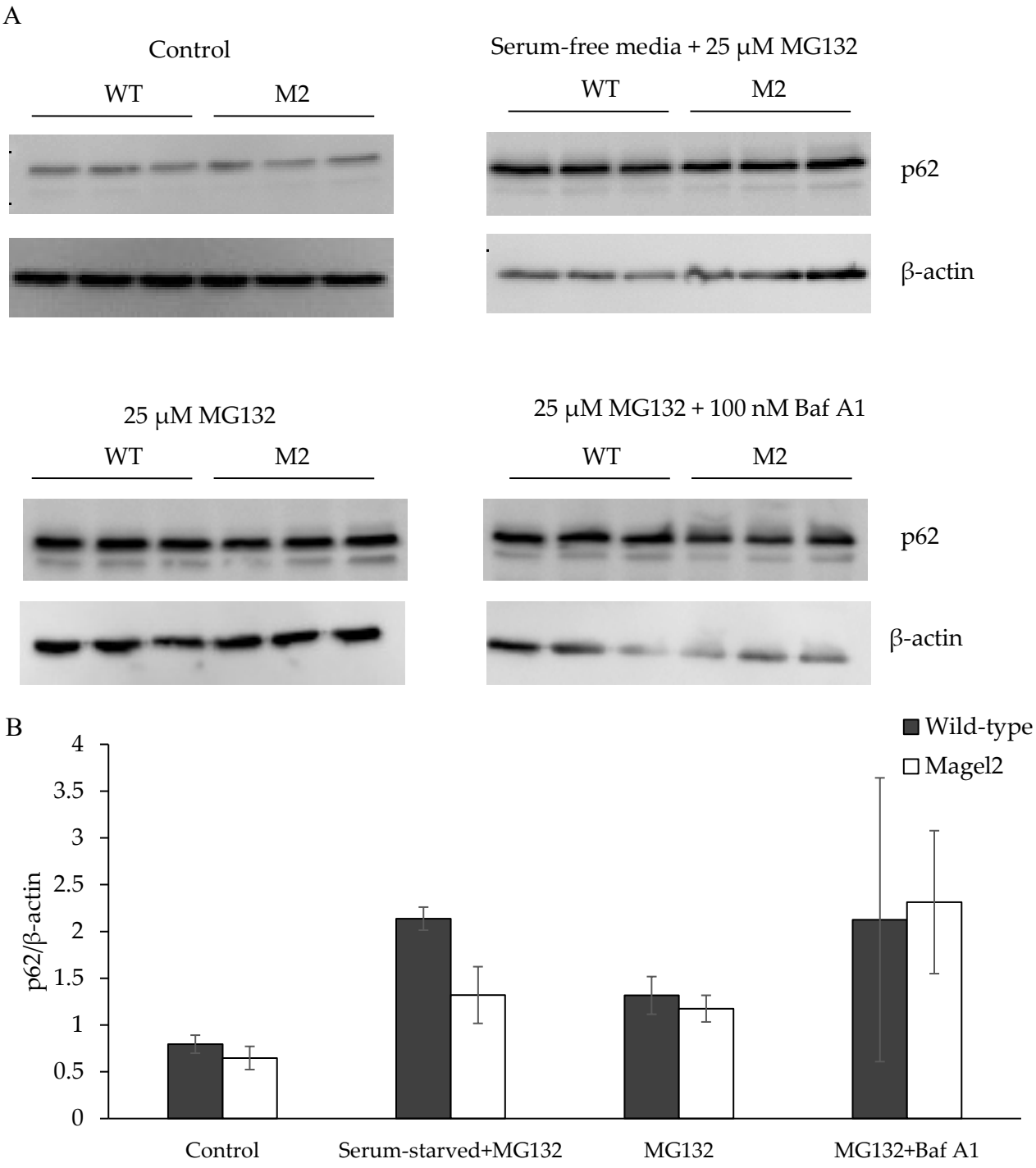

Figure 3.5 p62 expression in primary MEFs treated with 25 μM MG132 and 100 nM Baf A1 for 6 hours. A) Blots showing p62 expression in WT and *Magel2*-null (M2) primary MEFs treated with 4 different treatments. B) Quantification of p62 bands in A. WT N=3, Magel2 N=3.

3.2 p62 and ubiquitin levels are dysregulated and abnormal in POMC neurons of *Magel2*-null mice

To better understand autophagy at the neuronal level in *Magel2*-null mice, I measured p62 and ubiquitin expression in sections of arcuate nucleus from mice expressing GFP in POMC neurons (Figure *3.6* and Figure 3.7). I found that all POMC neurons were also positive for p62 and approximately 96% of POMC neurons were positive for ubiquitin in sections of arcuate nucleus from WT mice (Figure *3.6*B and Figure 3.7B). However in *Magel2*-null mice, only 70% of POMC neurons were also positive for p62 and 59% were positive for ubiquitin ($P<0.002$, comparing between genotypes by Fisher Exact test, Figure *3.6*B and Figure 3.7B). Furthermore, p62- and GFP-double positive neurons from *Magel2*-null mice had reduced p62 intensity compared to double positive neurons from WT mice ($P<0.05$, Mann Whitney test, Figure *3.6*C). Similar results were obtained for ubiquitin intensity in ubiquitin- and GFP-double positive neurons ($P=0.0005$, Mann Whitney test, Figure 3.7C). I also tried to determine whether there was any abnormality in p62 and ubiquitin expression earlier in development using primary neonatal hypothalamic neurons. However, GFP expression was too low and I could not differentiate between POMC-positive neurons and other neurons (Figure *3.8*). Even though I could not detect a significant change in p62 and ubiquitin levels on immunoblots of protein lysates from hypothalamus of *Magel2*-null compared to WT mice, the immunohistochemistry results suggest that only certain neuronal populations in the hypothalamus have an alteration in autophagic degradation, including POMC neurons. In summary, the loss of Magel2 leads to a decrease in p62 and ubiquitin levels in *Magel2*-null POMC neurons in the hypothalamus. Therefore, Magel2 is required to maintain normal autophagic degradation in POMC neurons, and perhaps in other neuronal populations not investigated here.

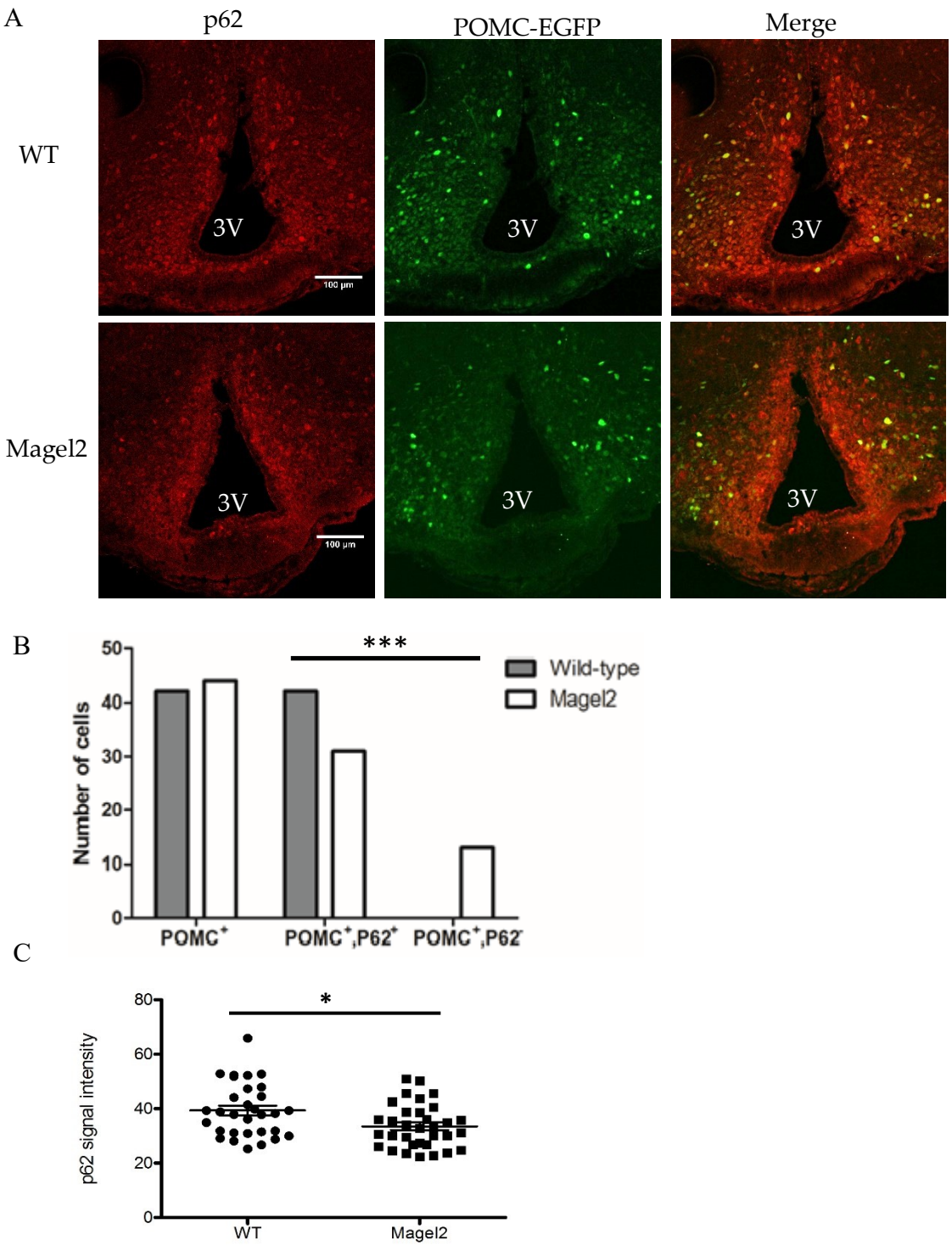

Figure 3.6 p62 expression in the arcuate nucleus of the hypothalamus. A) Detection of p62 (red) in the arcuate nucleus and EGFP (green) in POMC neurons by immunohistochemistry. Third ventricle (3V). B) Quantification of the number of POMC and p62 positive neurons (***P<0.0001, Fisher Exact test). C) Quantification of p62 signal intensity in double positive neurons. (*P=0.01, Mann Whitney test). N=1.

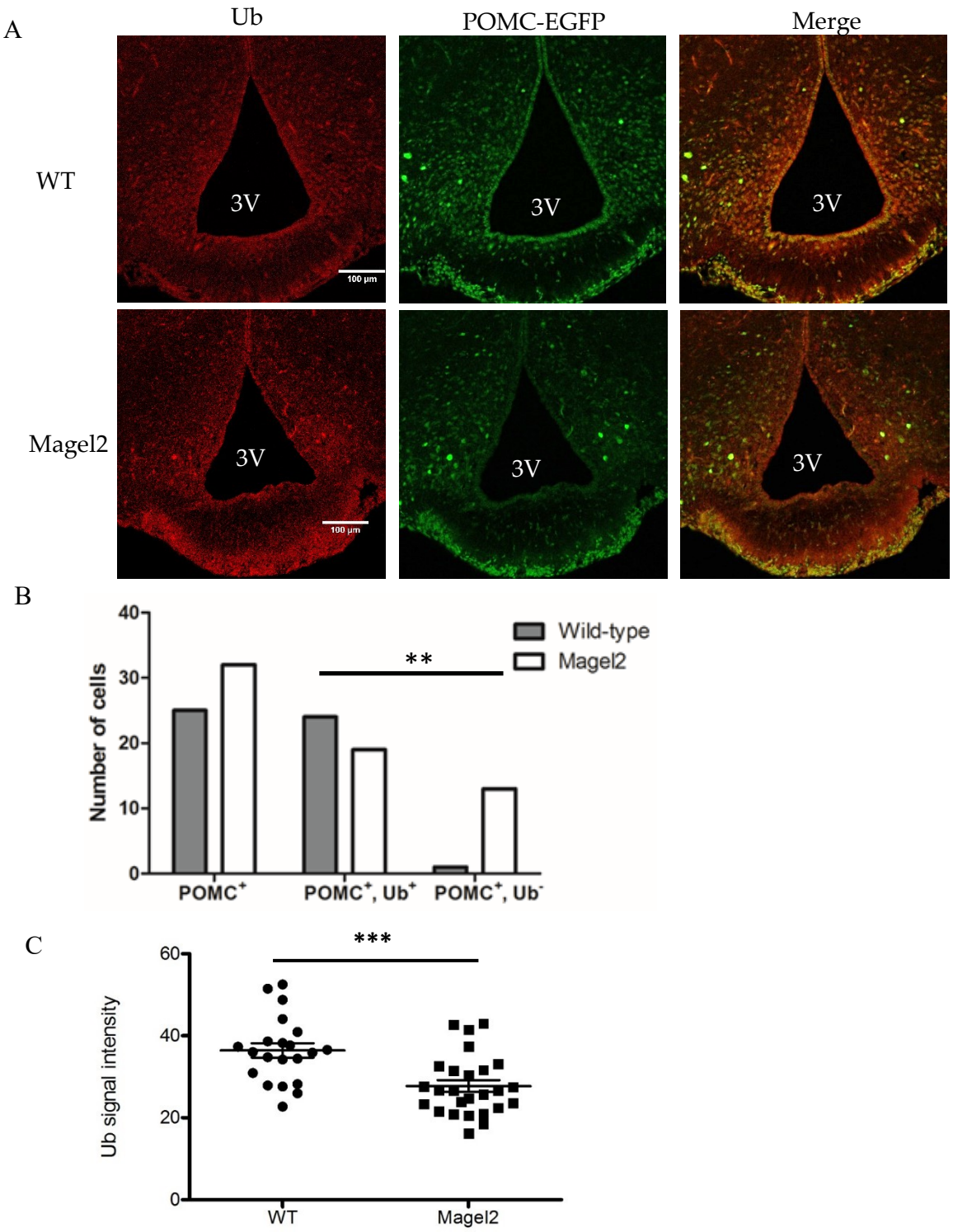

Figure 3.7 Ubiquitin expression in the arcuate nucleus of the hypothalamus. A) Detection of ubiquitin (Ub) (red) in the arcuate nucleus and EGFP (green) in POMC neurons by immunohistochemistry. Third ventricle (3V). B) Quantification of the number of POMC and Ub positive neurons (**P=0.0015, Fisher Exact test). C) Quantification of Ub signal intensity in double positive neurons (***P=0.0005, Mann Whitney test). N= 1.

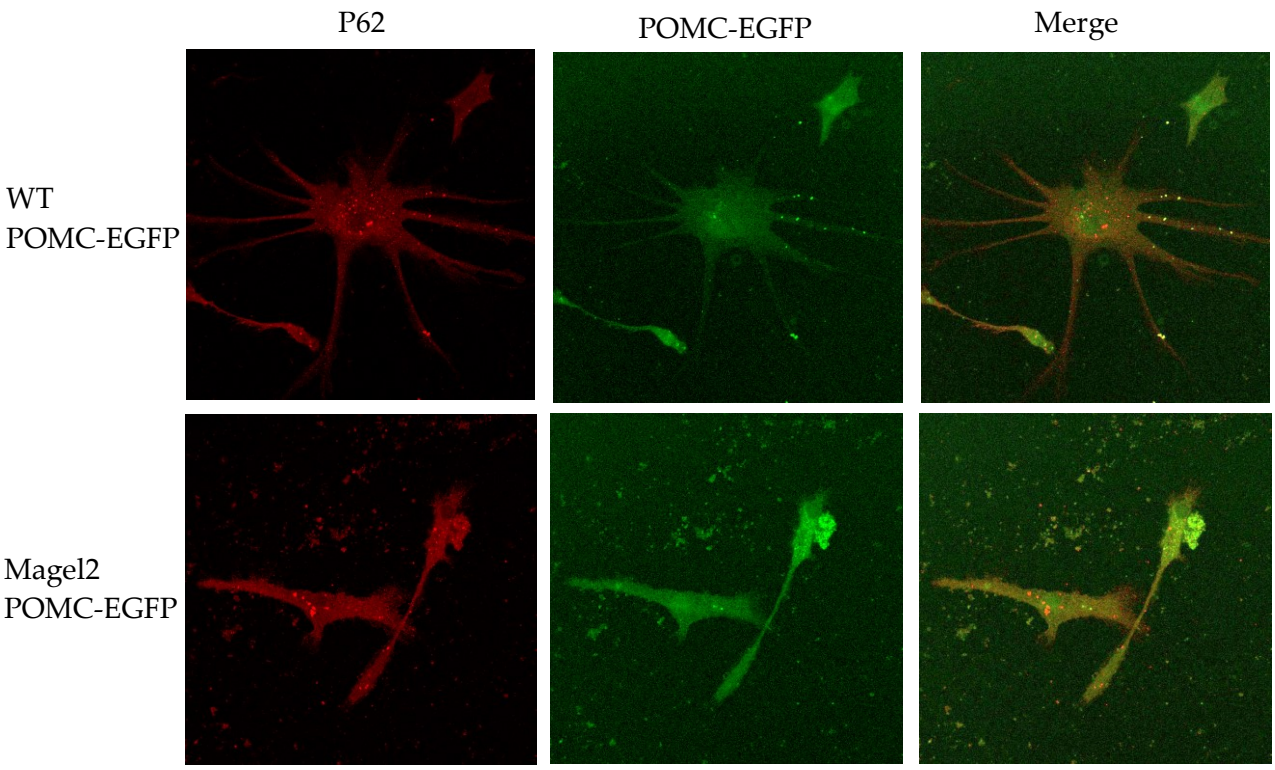

Figure 3.8 p62 (red) and EGFP expression in neonatal primary hypothalamic neurons from both WT POMC-EGFP and *Magel2*-null POMC-EGFP brain. The green colour seen in POMC-EGFP panel is likely background fluorescence since all cells are positive for the green colour.

3.3 *Magel2* expression decreases over time in muscle cells

Musculoskeletal phenotypes such as severe arthrogryposis, hypotonia, bilateral club foot, camptodactyly and hip dysplasia are seen in neonates with inactivation of *MAGEL2* alone, suggesting that loss of *MAGEL2* might have significant effects on muscle formation and development in children with Schaaf-Yang syndrome (Schaaf *et al.*, 2013; Mejlachowicz *et al.*, 2015). In the developing mouse, *Magel2* expression was mostly restricted to the central nervous system, but it is also expressed in the tongue, genital tubercle, midgut region, dorsal root ganglia and neurons innervating limbs and torso muscles (Lee *et al.*, 2000; Kozlov *et al.*, 2007). To better understand the role of *Magel2* in muscle, I measured *Magel2* expression in mouse muscle at different ages (P2, P12 and adult) by quantitative RT-PCR (qRT-PCR). Moderate levels of *Magel2* expression were detected (average Ct=24.2) at P2, but *Magel2* expression was reduced 8-fold at P12 and was undetectable in adult muscle (Figure *3.9*). I was also interested in determining the expression levels of *MAGEL2* in human muscle. In human, *MAGEL2* expression was detected at low levels in control fibroblasts and in the skeletal muscle of a mid-gestation fetus (Boccaccio *et al.*, 1999; Mejlachowicz *et al.*, 2015). I measured human *MAGEL2* expression in control fibroblasts transduced with MyoD-expressing construct then cultured in differentiation media to induce differentiation into myotubes (Saito *et al.*, 2010). I observed *MAGEL2* expression in control fibroblasts and throughout 18 days of the differentiation process to myotubes (Figure *3.10*). In addition, I also tested whether *MAGEL2* is expressed in immortalized human myoblasts that were differentiated into myotubes. *MAGEL2* is not expressed in the human myoblasts and in the myoblasts that were differentiated for 3 and 6 days (Figure *3.11*). However, *MAGEL2* expression was detected after 9 days of differentiation and onwards. These results demonstrate that both human *MAGEL2* and mouse *Magel2* are expressed in muscle cells during muscle formation.

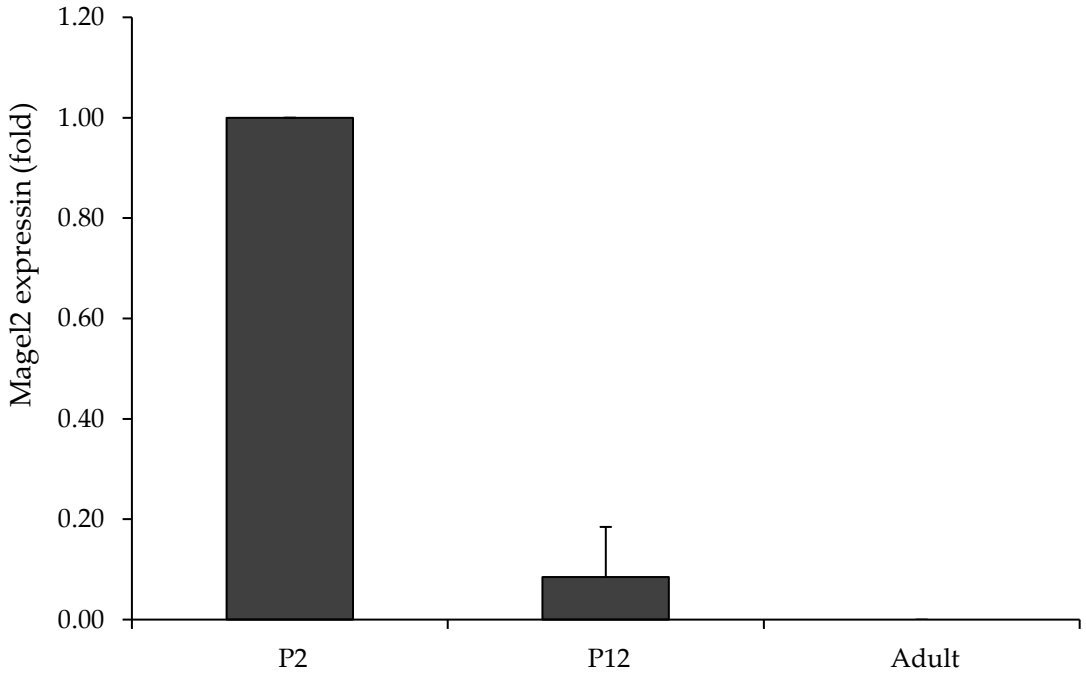

Figure 3.9 Quantification of *Magel2* expression by qRT-PCR in mouse muscle at different ages (P2, P12 and adult). *Magel2* expression was normalized to *Tbp* expression and was represented as a proportion of the expression at P2. N=3.

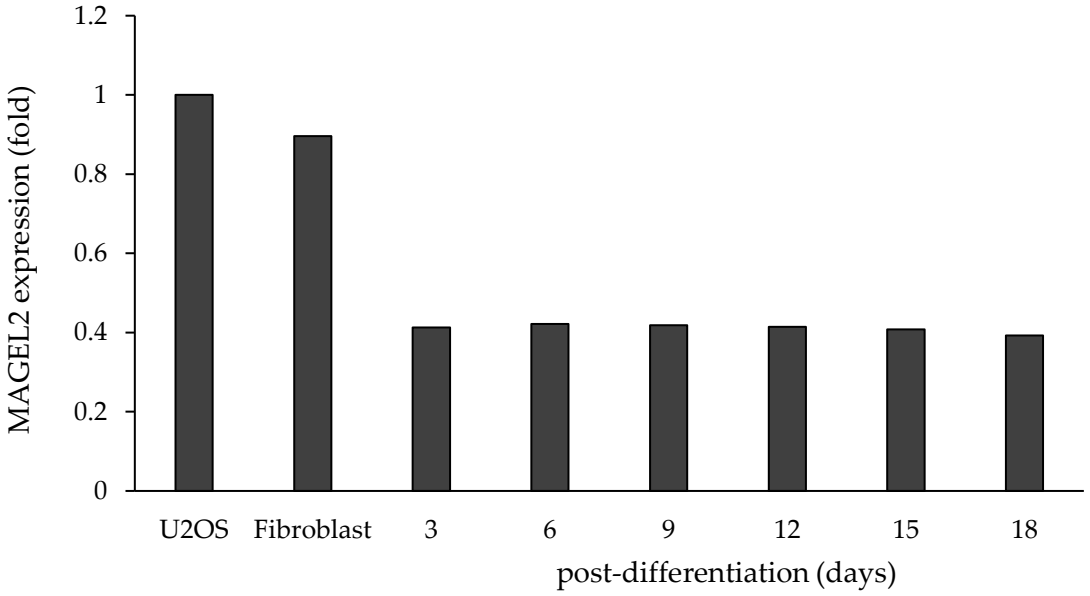

Figure 3.10 Quantification of *MAGEL2* expression in human fibroblasts and MyoD-transduced fibroblasts that are differentiating into myotubes up to 18 days. *MAGEL2* expression was normalized to *SDHA* expression and was represented as a proportion of endogenous *MAGEL2* expression in U2OS cells. N=1

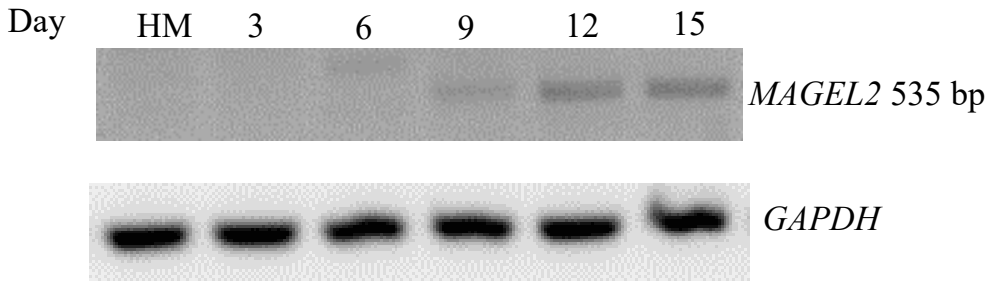

Figure 3.11 Human *MAGEL2* in human myoblasts (HM) and human myoblasts that are differentiating into myotubes up to 16 days, by non-quantitative RT-PCR. *GAPDH* expression was used as a positive control for the RT-PCR. N=1

3.4 Reduced muscle mass, changes in fiber size, but unaltered histology in *Magel2*-null muscle

Children and adults with PWS have increased fat mass and reduced lean mass, which correlates with reduced physical activity and low energy expenditure (Schoeller *et al.*, 1988; Goldstone *et al.*, 2002; Bekx *et al.*, 2003; Eiholzer *et al.*, 2004). Similarly, *Magel2*-null mice have altered body composition with the levels of adipose tissue inversely proportional to lean mass, recapitulating abnormalities of body composition seen in people with PWS (Bischof *et al.*, 2007). To better understand the cause of reduced lean mass, I dissected and weighed 3 different muscle groups (gastrocnemius-soleus-plantaris (GSP), quadriceps (Q), tibialis anterior (TA)) to ascertain whether reduced lean mass is associated with alteration in mass or histology of individual muscles (Figure *3.12*A). Muscle weight was reduced by 10.5% for GSP, 13.7% for Q and 18% for TA in *Magel2*-null male compared to WT male mice (Figure *3.12*B). A similar trend was observed for muscle weight in *Magel2*-null females with a reduction of 7% for GSP, 9% for Q and 10% for TA when compared to WT mice (Figure *3.12*C). There was a significant effect of both genotype (less mass in *Magel2*-null compared to WT, male $P=0.002$, female $P<0.05$, two-way ANOVA) and muscle type (highest mass reduction in TA compare to Q and GSP, male and female $P<0.0001$, two-way ANOVA) on muscle mass. These results are consistent with the total reduction in lean mass observed in *Magel2*-null mice and people with PWS, even though the reduction in muscle mass is not large.

I also examined the histology of gastrocnemius, soleus and tibialis anterior muscle by histochemistry to determine whether reduced muscle mass is accompanied by changes in muscle histology. I did not see any evidence of fatty infiltration, centrally nucleated fibers (regenerating muscles), irregularity in myofiber size, or presence of vacuolated fibers that would indicate muscle degeneration on muscle sections stained with hematoxylin and eosin (Figure *3.13*). These results suggest that muscle histology is grossly normal in *Magel2*-null mice. I expanded my study by determining whether reduced muscle mass is correlated with alteration in muscle fiber size. I visualized cell membranes by using antibody against dystrophin and labelled cell nuclei with DAPI, then measured the cross-sectional areas of the muscle fibers (Figure *3.14*A). I observed similar patterns of dystrophin staining between genotypes in both gastrocnemius and soleus sections. However, I found a smaller mean and median fiber size in gastrocnemius of *Magel2*-null mice compared to WT mice ($P=0.0001$, Mann-Whitney test) (Figure *3.14*B). Interestingly, the

opposite result was obtained from soleus section, in which I observed a larger mean and median fiber size in soleus of *Magel2*-null mice compared to WT mice ($P<0.0001$, Mann-Whitney test) (Figure *3.14*C). In summary, reduced lean mass seen in *Magel2*-null mice is accompanied by reduce muscle mass and shift in fiber size distribution, while the histology of the muscle is normal.

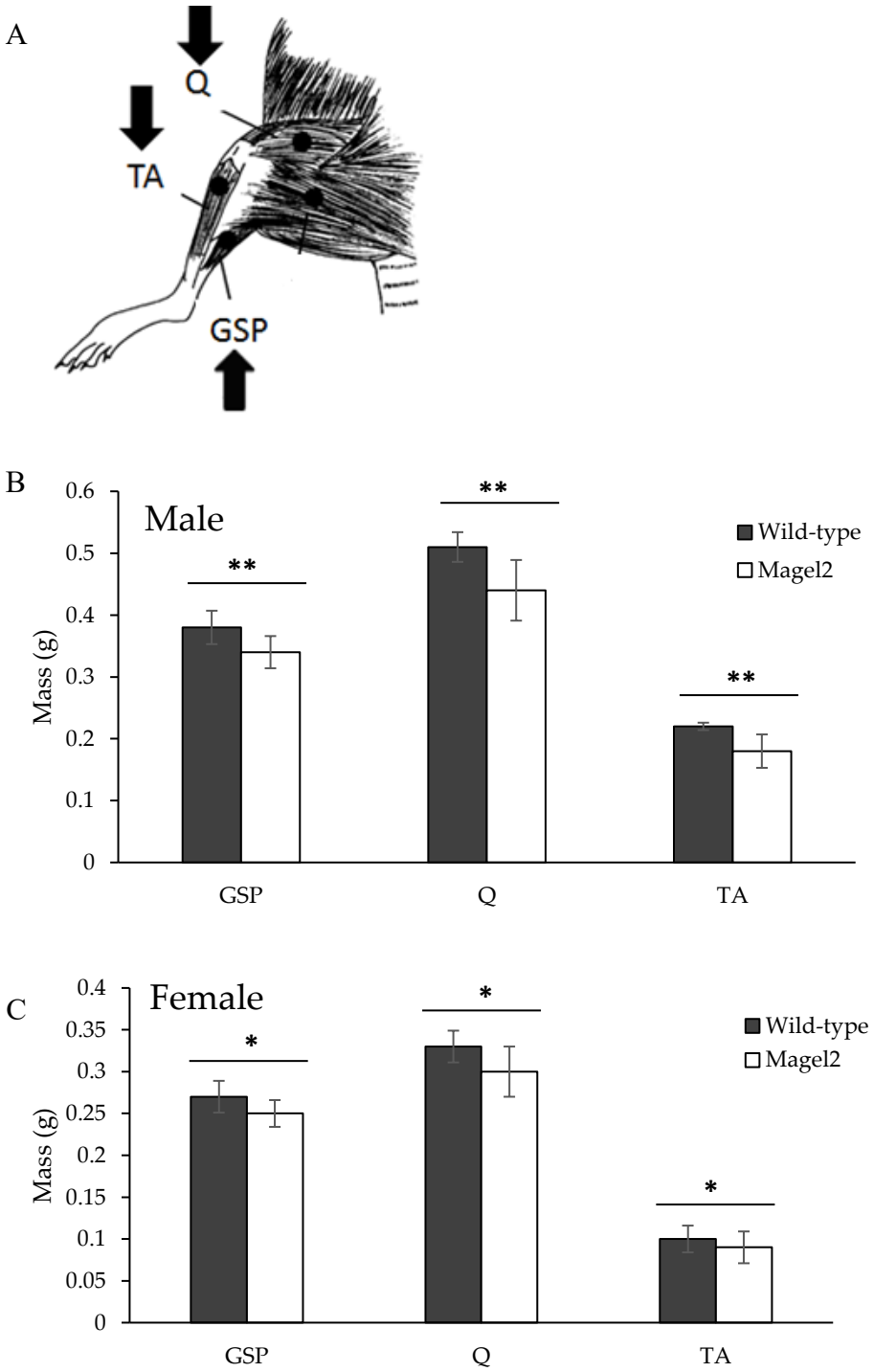

Figure 3.12 Muscle mass of individual muscle group. A) The position of gastrocnemius-soleus-plantaris (GSP), quadriceps (Q) and tibialis anterior (TA) muscle in the hind leg. B) Muscle mass of male mice. Two-way ANOVA, P=0.002 (mean±standard deviation (SD), WT N=3, Magel2 N=4). C) Muscle mass of female mice. Two-way ANOVA, P<0.05 (mean±SD , WT N=3, Magel2 N=6).

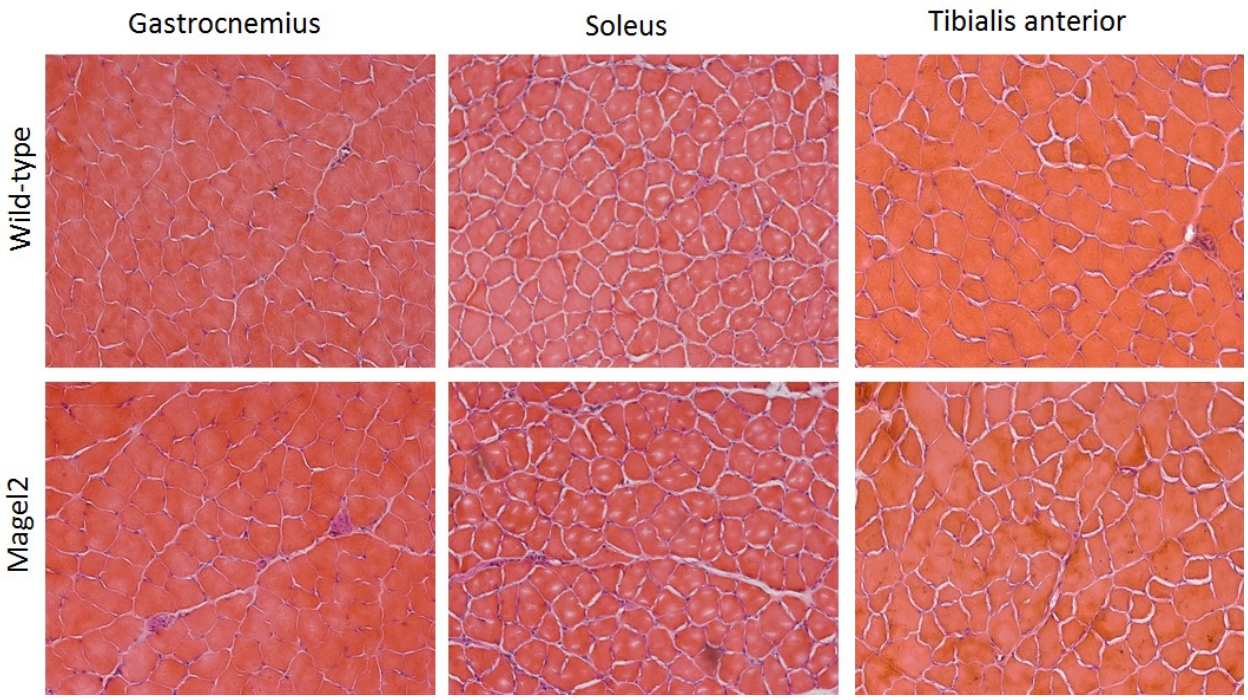

Figure 3.13 Hematoxylin and eosin histochemistry on gastrocnemius, soleus and tibialis anterior. There is no evidence of fatty infiltration or centrally nucleated fibers.

A

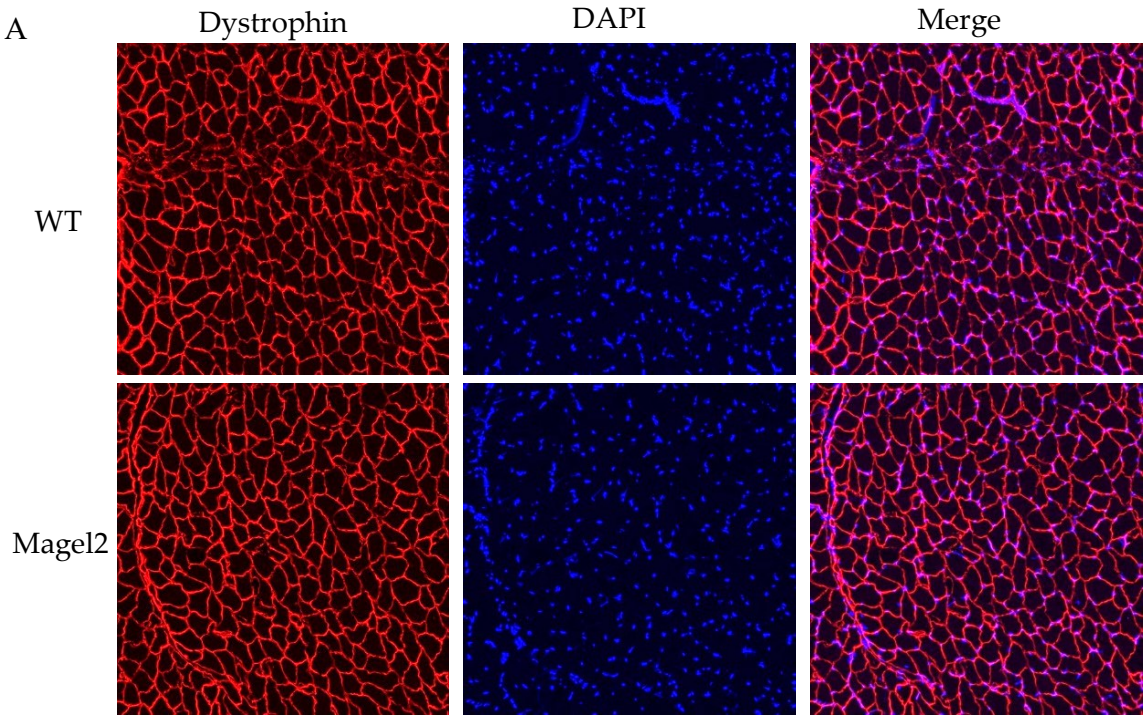
Dystrophin
DAPI
Merge
WT
Magel2

B

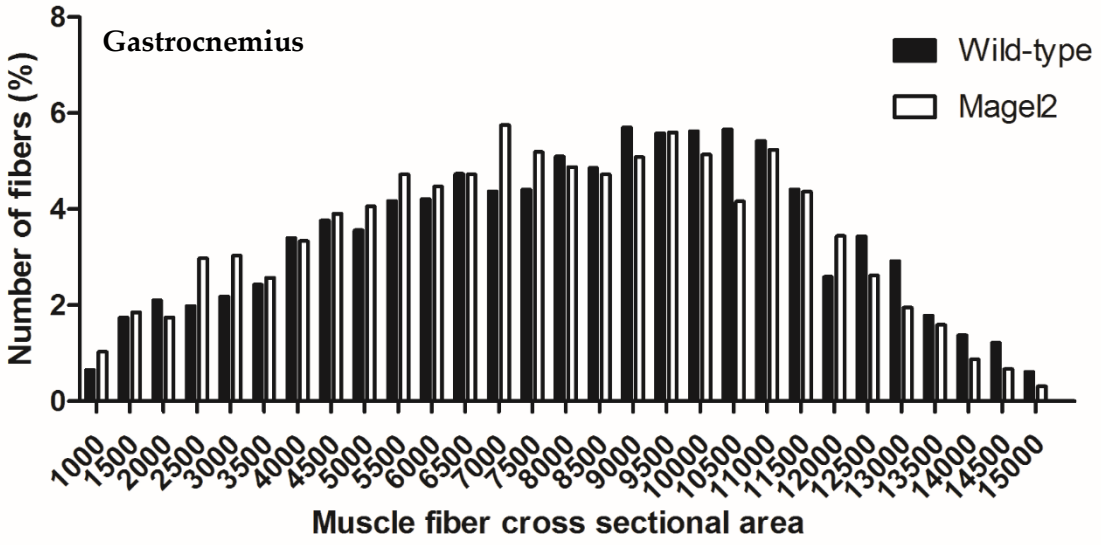
Gastrocnemius
Wild-type
Magel2
Number of fibers (%)
0
2
4
6
8
1000
1500
2000
2500
3000
3500
4000
4500
5000
5500
6000
6500
7000
7500
8000
8500
9000
9500
10000
10500
11000
11500
12000
12500
13000
13500
14000
14500
15000
Muscle fiber cross sectional area

C

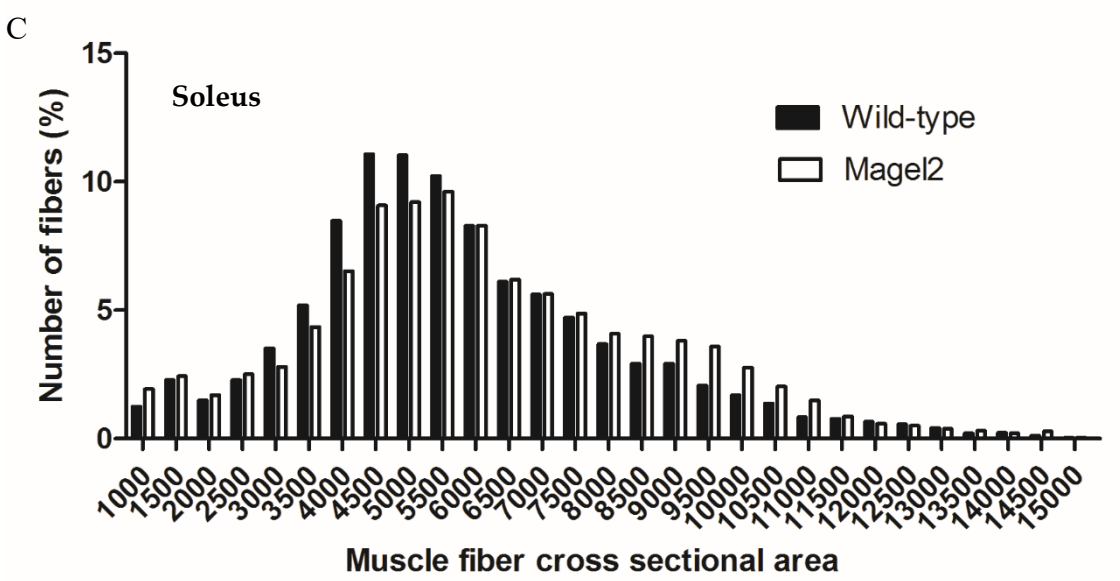

Figure 3.14 Fiber size distribution in gastrocnemius and soleus. A) Cell nuclei were labelled with DAPI and cell membranes with anti-dystrophin antibody. B) Fiber size distribution in gastrocnemius shows a shift towards smaller fiber size in the *Magel2*-null mice. N=3. C) Fiber size distribution in soleus shows a shift towards larger fiber size in the *Magel2*-null mice. N=3.

3.5 Induction of atrophy genes and altered autophagy in *Magel2*-null muscle

I also tested whether the reduced lean mass is associated with *Magel2*-null skeletal muscle (GSP) undergoing atrophic processes, by measuring the expression of atrogenes, which are atrophy-related genes that are transcriptionally dysregulated under atrophy-inducing conditions (Bonaldo and Sandri, 2013). MAFbx/atrogin 1 and MuRF1/Trim63 are two major atrogenes that encode E3 ubiquitin ligases, important components of ubiquitin-proteasome pathway in muscle (Bodine and Baehr 2014; Bodine et al. 2001). I observed a significant effect of both genotype (higher expression in *Magel2*-null muscle compared to WT muscle, P=0.006, two-way ANOVA) and age (higher in adult compared to P2, P<0.0001, two-way ANOVA) on *MuRF1* expression (Figure 3.15A). The difference in *MuRF1* expression between genotypes was only statistically significant in the adult samples (P<0.05, Bonferroni posttest). For *MAFbx* expression, there was a significant effect of age (higher in adult compared to P2, P<0.0001, two-way ANOVA) and an interaction between genotype and age (P=0.05, two-way ANOVA) (Figure 3.15B). However there was no significant difference between genotypes for *MAFbx* expression at either age. These results show that *Magel2*-null adult muscle went through atrophic processes, but atrophy was not detected in *Magel2*-null muscle at postnatal day 2.

Basal autophagy is vital for maintaining muscle mass, and altered autophagy in skeletal muscle triggers muscle loss and induces atrophy (Masiero *et al.*, 2009; Masiero and Sandri, 2010; Neel *et al.*, 2013; Sanchez *et al.*, 2014). I expanded my study by looking at the autophagy-lysosome system in *Magel2*-null muscle. Skeletal muscle myofibers normally undergo low levels of autophagy, but conditions such as stress and nutrient starvation can lead to increased autophagy in the muscle (Kuma *et al.*, 2004; Mizushima *et al.*, 2004). I measured the accumulation of ubiquitinated protein by assessing signal intensity of p62 aggregates in muscle fibers of adult mice under either fed or fasted (24 hours) conditions. As expected, there was a higher average signal intensity of p62 aggregates observed in fasted WT soleus muscles compared to fed WT soleus muscles (Figure *3.16*A). Surprisingly, fed *Magel2*-null soleus muscles had higher signal intensity of p62 aggregates compared to fed WT soleus muscles, and similar signal intensity of p62 aggregates to fasted WT soleus muscles (Figure *3.16*A). I did not observe any difference in the signal intensity of p62 aggregates in relation to feeding state or genotype for tibialis anterior muscle sections (Figure *3.16*B). In summary, my results suggest muscle atrophy, as detected by

the upregulation of *MuRF1* expression in adult *Magel2*-null muscle and by the increase in p62 aggregation in the fed *Magel2*-null soleus muscle compared to WT soleus muscle.

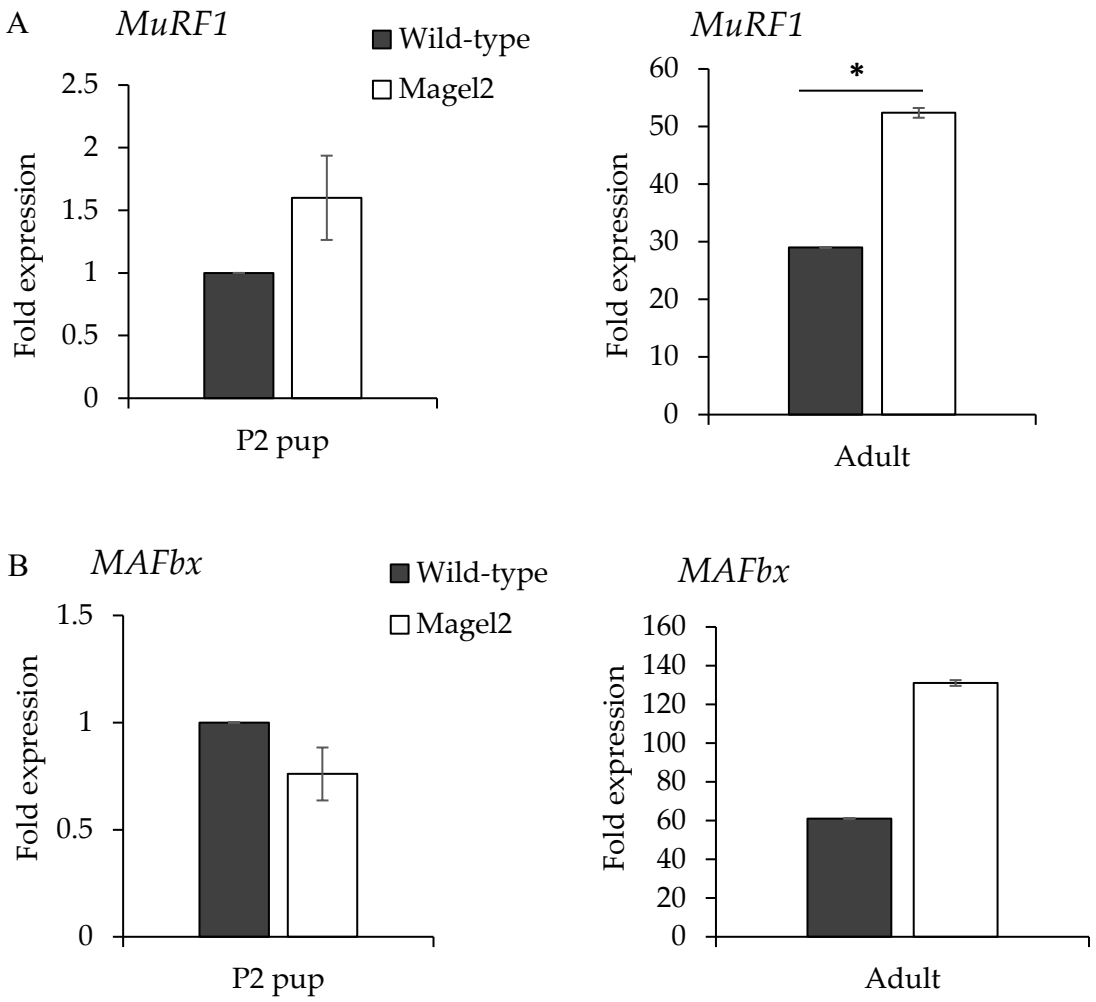

Figure 3.15 Expression of atrogenes in P2 and adult muscles. A) *MuRF1* expression was normalized to *Tbp* and was represented as a proportion of the endogenous expression in wild type sample (*P=0.05, Bonferroni posttest). B) *MAFbx* expression was normalized to *Tbp* expression and was represented as a proportion of endogenous expression in wild type sample. N=3

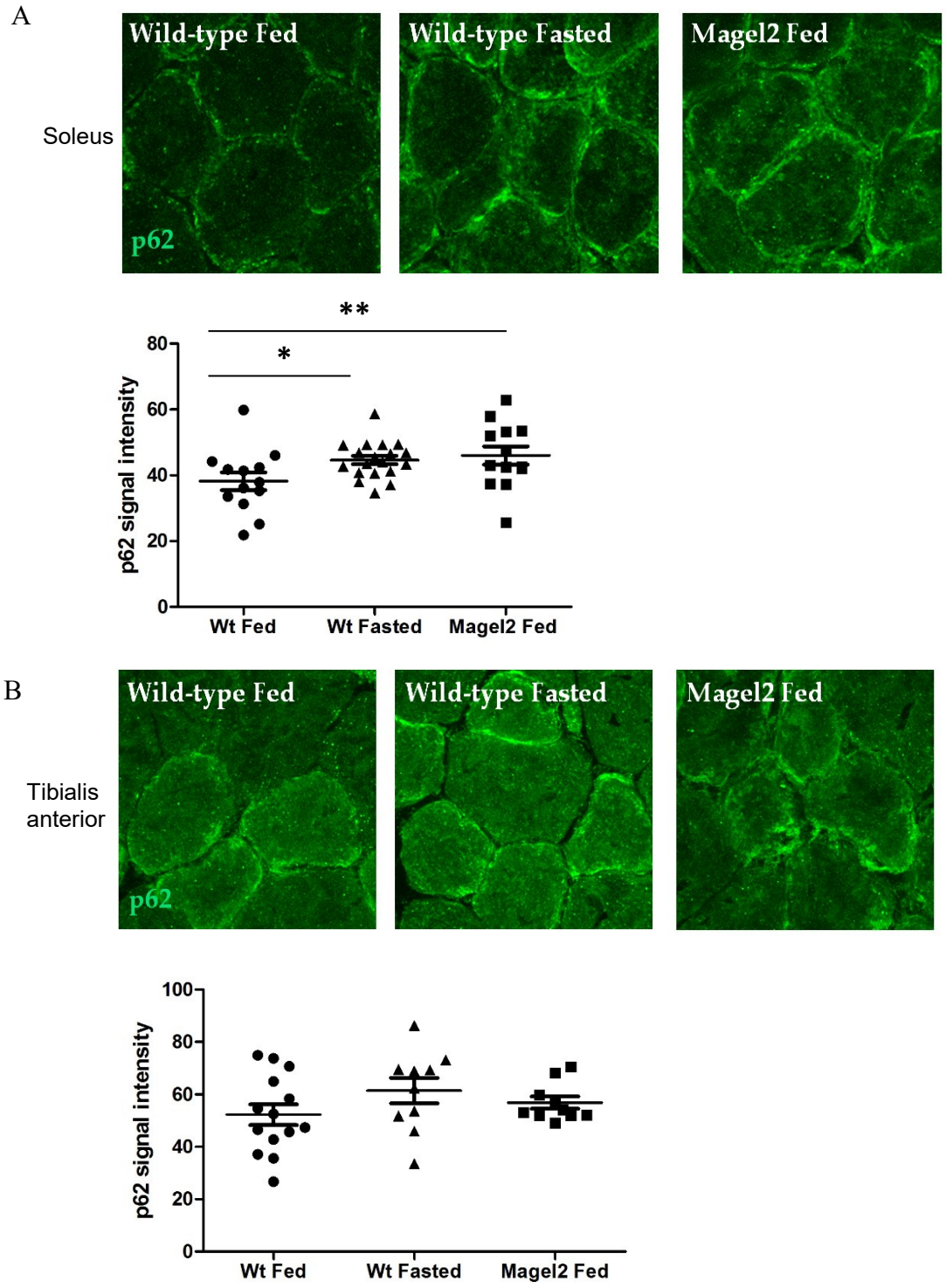

Figure 3.16 p62 expression in fed and fasted (24 hours) muscle. A) Higher signal intensity of p62 aggregates in fed *Magel2*-null soleus sections compared to fed WT soleus sections, and similar to fasted WT soleus sections (*P=0.02, **P=0.04, Mann-Whitney test). B) No feeding or genotype-dependent difference in the signal intensity of p62 aggregates in tibialis anterior sections. N=2-3

4 Chapter 4: Discussion

I hypothesized that the loss of *MAGEL2* contributes to obesity in PWS because of autophagy impairment in the anorexigenic POMC neurons in the hypothalamus, and a similar impairment of autophagy causes severe hypotonia and other musculoskeletal abnormalities seen in PWS and Schaaf-Yang Syndrome (Cassidy *et al.*, 2012; Schaaf *et al.*, 2013; Torrado *et al.*, 2013). Infants with PWS are commonly born underweight but start to gain weight after the age of 2, followed by significantly increased body weight, hyperphagia and lack of satiety at the age of 8 (Cassidy *et al.*, 2012). Hyperphagia leading to obesity seen in children with PWS is believed to be caused by hypothalamic dysfunction resulting in high appetite and lower energy usage (Butler *et al.*, 2007; Cassidy *et al.*, 2012). A mouse model lacking Magel2 was created by replacing the ORF of the *Magel2* gene with an in-frame LacZ knock-in expression cassette, to recapitulate these phenotypes and study the role of Magel2 loss (Bischof *et al.*, 2007). Mice lacking *Magel2* expression have hypothalamic dysfunctions including endocrine defects, circadian defects, infertility, increased adiposity and insensitivity towards adipocyte-derived plasma hormone leptin (Bischof *et al.*, 2007; Kozlov *et al.*, 2007; Mercer and Wevrick, 2009; Mercer *et al.*, 2013; Pravdivyi *et al.*, 2015), indicating this mouse model was suitable to study how the loss of Magel2 contributes to PWS. At the intracellular level, MAGEL2 binds to the E3 ubiquitin ligase TRIM27 and this MAGEL2-TRIM27 complex enhances nucleation of endosomal F-actin and retromer-mediated retrograde transport (Doyle *et al.*, 2010; Hao *et al.*, 2013). In addition to the role of MAGEL2 in protein trafficking reported by Hao *et al*, I predicted that MAGEL2 might also have role in protein degradation. Interestingly, in this thesis project, I discovered that *Magel2* specifically plays a role in regulating autophagy in the hypothalamic POMC neurons.

Food intake and energy expenditure are centrally regulated by two main hypothalamic neurons: anorexigenic POMC neurons and orexigenic agouti-related peptide (AgRP)/NPY neurons (Elmquist *et al.*, 2005; Williams and Elmquist, 2012). Many studies have reported the importance of a balance in autophagic rate in these neurons to regulate energy homeostasis, body weight and food intake (Kaushik *et al.*, 2011, 2012; Coupé *et al.*, 2012; Quan *et al.*, 2012). Mice lacking autophagy in POMC neurons had increased body weight, adiposity and an accumulation of p62, conjugated LC3-II and ubiquitinated proteins (Coupé *et al.*, 2012; Kaushik *et al.*, 2012; Quan *et al.*, 2012). In contrast, mice lacking autophagy in AgRP neurons had reduced body weight, increased α-MSH and increased lipid breakdown (Kaushik *et al.*, 2011). Based on these findings,

I determined the expression of autophagy markers, LC3, p62 and ubiquitinated proteins by immunoblotting. Results from the experiments show that basal autophagy occurs similarly in the hypothalamus and primary MEFs of WT and *Magel2*-null mice (Figure *3.1*-Figure *3.5*). In addition, blockage of lysosomal degradation by Baf A1 treatment in *Magel2*-null primary MEFs increased the levels of conjugated LC3-II and p62 protein to a similar extent as seen in WT primary MEFs, suggesting autophagosome formation and clearance are normal in *Magel2*-deficient primary MEFs (Figure *3.3*). Moreover, proteasomal degradation is not affected by *Magel2* deficiency in primary MEFs as seen from an indistinguishable accumulation of conjugated LC3-II and p62 proteins in WT and *Magel2*-null primary MEFs during proteasomal inhibition (Figure *3.4* and Figure *3.5*).

However, mice with deletion of Atg7, a gene required for autophagosome formation specifically in the POMC neurons, have increased adiposity, while increased adiposity is also found in *Magel2*-null mice (Bischof *et al.*, 2007; Coupé *et al.*, 2012). Disruption of autophagy by deletion of Atg7 in POMC neurons is accompanied by an accumulation of p62 and ubiquitinated proteins (Coupé *et al.*, 2012). In addition, deletion of p62 in these neurons also leads to obesity in mice (Harada *et al.*, 2013). Autophagy disruption in POMC neurons due to either increased or decreased p62 expression causes increased adiposity in mice. The similar increase in adiposity observed in mice lacking Atg7 in POMC neurons and in mice lacking *Magel2* suggests that Magel2 could regulate body composition by maintaining normal autophagic process in POMC neurons. In order to determine whether *Magel2* plays important role in regulating autophagy specifically in POMC neurons, p62 and ubiquitinated protein expression were examined in *Magel2*-null brain sections. Immunohistochemistry analysis demonstrates reduced p62 and ubiquitinated protein expression in the POMC neurons of *Magel2*-null mice compared to WT mice (Figure *3.6* and Figure 3.7). POMC neurons have restricted distribution in the CNS with POMC cell bodies mainly present in the arcuate nucleus of the hypothalamus and in the nucleus of the tractus solitarus (NTS) in the brain stem (Coupe and Bouret, 2013). In addition, the number of POMC neurons was reduced in the hypothalamic arcuate nucleus and its projection to PVN was impaired in mice lacking *Magel2* expression (Mercer *et al.*, 2013; Pravdivyi *et al.*, 2015). The observation that POMC neurons account for a small subset of neurons in the hypothalamus and reduced number of POMC neurons in *Magel2*-deficient hypothalamus may explain the difference in the levels of autophagy seen in protein lysates collected from hypothalamus and on the arcuate nucleus sections.

The small difference in the autophagy levels between genotypes was not readily observed in the whole hypothalamus protein lysates that contain protein from other neuronal populations, which suggests that *Magel2* is required to maintain normal autophagy clearance only in the small population of POMC neurons or possibly in other neurons not investigated here.

Autophagy occurs in nearly all cell types and emerging reports suggest that the regulation of autophagy is cell type- and tissue-specific (Mizushima *et al.*, 2004). Starvation induces autophagy in most of tissues including liver, heart, pancreas, gastrocnemius, soleus, kidney and thymus, but these tissues respond differently to starvation (Mizushima *et al.*, 2004). Autophagy disruption (seen by reduction of conjugated LC3-II and p62 proteins) is not apparent in *Magel2*-null primary MEFs while it was seen in POMC neurons lacking *Magel2* expression, suggesting a differential regulation of autophagy by *Magel2* in these two cell types. In addition, the degree of vulnerability towards autophagy dysregulation varies significantly among different neuronal types. In a mouse model, deletion of Atg5/Atg7 in Purkinje cells causes decreased number of Purkinje cells and increased apoptosis in mice lacking Atg5/Atg7 (Hara *et al.*, 2006; Komatsu *et al.*, 2007b). Conversely, deletion of Atg7 in POMC neurons does not alter POMC neuron survival as observed by normal number of POMC neurons and absence of TUNEL-positive cells, although there are reduced axonal projections in mice lacking Atg7 (Coupé *et al.*, 2012; Kaushik *et al.*, 2012). Reduction of POMC axonal projections to the PVN in mice lacking *Magel2* expression is highly correlated with the alteration in the autophagy, whereas no alteration of apoptosis was detected in this study (Pravdivyi *et al.*, 2015 and Figure *3.16*).

I also determined that *Magel2* is required for muscle strength and regulating muscle mass. People with PWS have abnormal body composition with increased fat mass but reduced muscle mass that can be observed early in infancy (Reus *et al.*, 2011). Central hypotonia is common in infancy leading to difficulty sucking and failure to thrive (Cassidy *et al.*, 2012). Hypotonia improves over time, however it persists until adulthood causing individuals to remain mildly hypotonic. Infants with PWS have reduced muscle strength and children with PWS have reduced lower maximal muscle force and power relative to body weight (Edouard *et al.*, 2012; Reus *et al.*, 2013). In addition, mice lacking *Magel2* have decreased muscle mass and age-dependent reduction of grip strength (Bischof *et al.*, 2007; Kamaludin *et al*., manuscript submitted). Necdin, which is closely related to Magel2, is expressed in the myogenic progenitor cells and is important for muscle differentiation and muscle regeneration (Deponti *et al.*, 2007; Bush and Wevrick, 2008). In order

to determine if Magel2 has similar function as Necdin, human MyoD-transduced fibroblasts were differentiated into myotubes. I determined that *MAGEL2* is expressed in the healthy human fibroblasts and throughout the differentiation process to myotubes (Figure *3.10*). *MAGEL2* expression was also observed in immortalized human myoblasts differentiating into myotubes (Figure *3.11*). These results suggest that *MAGEL2* could regulate the differentiation of myoblasts or possibly has function similar to Necdin in muscle regeneration. In mouse, *Magel2* expression is detected in the muscle early after birth, but *Magel2* expression is reduced over time and is undetectable in adult muscle (Figure *3.9*), suggesting that *Magel2* might be more important for early developmental of skeletal muscle. Further experiments are needed to establish the role of Magel2 protein in myogenic differentiation and regeneration.

In addition to reduced grip strength found in mice lacking *Magel2* (Kamaludin *et al*,. manuscript submitted), I also observed decreased muscle mass in both male and female mice lacking *Magel2* (Figure *3.12*). The difference in muscle mass between WT muscle groups and *Magel2*-null muscle groups is bigger in male mice compared to female mice. Testosterone, a key reproductive hormone, increases muscle mass, strength, and endurance. Testosterone also induces hypertrophy of muscle fibers (Kadi, 2008) and muscle regeneration in both old and young mice is improved in the presence of testosterone (Serra *et al.*, 2013). Further, testosterone levels were significantly lower in *Magel2*-null male mice compared to WT male mice (Mercer and Wevrick, 2009). These findings suggest that lower levels of testosterone in *Magel2*-null male mice led to higher reduction in muscle mass in contrast to less reduced muscle mass seen in *Magel2*-null female mice. Adding to this, I also determined that reduced muscle mass in mice lacking *Magel2* is accompanied by changes in the distribution of muscle fiber cross-sectional areas (Figure *3.14*). Fiber cross-sectional area shifted towards smaller fiber size in gastrocnemius and shifted towards larger fiber size in soleus.

Decreased muscle mass and a shifted fiber size distribution are not only observed in *Magel2*-null mice, but these changes were also reported in a genetically obese (ob/ob) mouse model (Kemp *et al.*, 2009). Muscle analysis demonstrated reduced muscle mass in both fast- and slow-twitch muscles of ob/ob mice compared to control lean mice (Kemp *et al.*, 2009). The smaller mean cross-sectional area of fast-twitch muscles was due to decreased in fiber size, which led to smaller portion of type IIB fibers and larger portion of hybrid fibers, type IID/X + IIB (Kemp *et al.*, 2009). However, no significant difference was observed between the mean cross-sectional area of slow-

twitch muscle from ob/ob and lean control mice. Studies on patients with type 2 diabetes and patients with metabolic syndrome (presenting with central obesity with dyslipidemia, hypertension and hyperglycemia) reported a significant inverse relationship between the proportion of type I fiber and the amount of adipose tissue (Oberbach *et al.*, 2006; Stuart *et al.*, 2013). Similarly, obesity could contributes to the morphological alteration in *Magel2*-null muscle with respect to both muscle mass and fiber distribution. Despite changes in muscle fiber size distribution that results in smaller mean cross-sectional area in *Magel2* gastrocnemius and larger mean cross-sectional are in *Magel2* soleus, there was no evidence of muscle degeneration, regeneration, fatty infiltration or presence of vacuolated fibers seen in histological analysis of *Magel2*-null muscles (Figure *3.13*). Muscle histology analysis that could have identified muscle degeneration, regeneration and other morphological changes on ob/ob mice and patients with type 2 diabetes were not reported in those studies (Oberbach *et al.*, 2006; Kemp *et al.*, 2009; Stuart *et al.*, 2013). Further experiments are needed to determine whether there is a change in fiber types or a change in the size of the each fiber types in *Magel2*-null muscles.

Other than changes in muscle mass, changes in muscle atrophy are also seen in muscle cells under conditions of obesity (Pellegrinelli *et al.*, 2015). Co-culture of human myoblasts with the obese visceral adipose tissue (VAT) adipocytes results in significant decrease in the expression of several muscle-specific genes, including the myogenic transcription factors myogenic differentiation 1 (MyoD1) and myogenin, the growth factor IGF-II, the sarcomeric protein titin and α sarcoglycan (Pellegrinelli *et al.*, 2015). In addition, exposure of myotubes to VAT adipocytes led to decrease protein levels of titin and disruption in the sarcomeric structure observed through decreased striated titin expression. The atrophy phenotypes seen in co-cultured myoblast and myotubes result from a reduction of the Akt/S6K/4E-BP1 signalling pathway that is responsible for protein synthesis, and they are not caused by alteration in *MuRF1* or *MAFbx* expression. However, the activation of cellular proteolytic systems including autophagy-lysosome and ubiquitin-proteasome pathways triggered by growth factors, cachectic factors, oxidative stress, energy stress and nutrient levels can also lead to muscle atrophy (Sandri, 2008). Both increased or decreased skeletal muscle autophagy due to genetic alterations and genetic modification in various genes including E3 ligases cause muscle atrophy in mice (Bonaldo and Sandri, 2013; Neel *et al.*, 2013). Increased expression of atrophy-related genes *MuRF1* and *MAFbx*, and an accumulation of

p62 aggregates have been observed in muscles undergoing atrophy (Masiero *et al.*, 2009; Bodine and Baehr, 2014).

To that end, I observed an increase in expression of *MuRF1* in adult *Magel2*-null muscle (Figure *3.15*). MuRF1 plays an important role in regulating degradation of myofibrillar proteins (Clarke *et al.*, 2007). Exposure to dexamethasone, a synthetic glucocorticoid that induces atrophy, results in decreased MHC and increased MuRF1 expression (Clarke *et al.*, 2007). MuRF1 interacts with MHC and is required for the ubiquitination of MHC. Mice lacking MuRF1 treated with dexamethasone do not show significant loss of MHC compared to WT treated with dexamethasone, but instead have a significant increase in MHC levels (Clarke *et al.*, 2007). These findings suggest that increased *MuRF1* expression in adult *Magel2*-null muscles but not in neonate *Magel2*-null muscles reflects a process by which adult muscle undergoes atrophy over time with increased degradation of myofibrillar proteins. There might be no alteration in protein synthesis as *MAFbx* expression was not affected in either neonate or adult *Magel2*-null muscles (Figure *3.15*), but this will require further study.

Increased *MuRF1* expression in adult *Magel2*-null muscles is also accompanied by increased p62 accumulation (Figure *3.16*). Mice with muscle-specific Atg7 deletion, in which autophagy is inhibited, also showed accumulation of p62 in the muscle (Masiero *et al.*, 2009). Increased accumulation of p62 was observed in soleus but not in tibialis anterior, suggesting that slow-twitch soleus muscles in *Magel2*-null mice are more vulnerable to autophagy alteration compared to fast-twitch tibialis anterior muscles. MuRF1 regulates clearance of MHC through proteasomal degradation (Clarke *et al.*, 2007) while p62 links targeted protein to autophagosome to be degraded through autophagy (Bjørkøy *et al.*, 2005). Upregulation of both MuRF1 and p62 in *Magel2*-null muscle (Figure *3.15* and Figure *3.16*) suggests increased protein degradation via both proteolysis pathways. Interestingly, the levels of p62 in *Magel2*-null muscle are opposite to the levels of p62 in *Magel2*-null POMC neurons. Higher levels of p62 in *Magel2*-null muscle, where basal autophagy is normally low in freely fed animals, and lower levels of p62 in *Magel2*-null POMC neurons, where basal autophagy is constitutively high, suggest cell type-specific regulation of autophagy by Magel2. *Magel2* is constitutively expressed in POMC neurons but only expressed early in muscle development postnatally. This suggests a continuous role of Magel2 in regulating neuronal autophagy, in contrast to its role in muscle that might be more important in early muscle development. However, the potential role of *Magel2* in regulating motor neuron function or

perhaps neuromuscular junctions that might lead to muscle phenotypes seen in *Magel2*-null mice remains to be investigated.

Future Directions

Further study needs to be done to fully elucidate the role of *Magel2* in regulating autophagy in neuronal cells and its connection to muscle function, as well as understanding the role of *MAGEL2* loss in contributing to obese and muscle phenotypes in PWS and Schaaf-Yang Syndrome. Further experiments are needed in order to address some unanswered questions including how Magel2 regulates the levels of autophagy in POMC neurons. As it is not clear if autophagy alteration is due to suppression of autophagy initiation or increase autophagy clearance, it will be helpful to investigate the role of Magel2 in regulating autophagy at the single neuron level. Since I already confirmed there was disruption of autophagy in *Magel2*-null mice, this project can be expanded into cultured cells and various manipulations can be introduced to establish the relationship between Magel2 and autophagy. For instance, GFP-LC3 can be transfected into GT1-7 mouse hypothalamic cell line that endogenously expresses Magel2. The expression of cytoplasmic GFP-LC3 and conjugated GFP-LC3 can be observed and compared between WT and Magel2-knockdown cells (by siRNA) by immunofluorescence or immunoblot. In addition, it will be interesting to find out whether knocking down Magel2 expression in GT1-7 cells will cause similar reduction in the levels of p62 and ubiquitinated proteins as seen in *Magel2*-null POMC neurons (Figure *3.6* and Figure 3.7). It would also be interesting to determine whether rescuing Magel2 expression in *Magel2*-knockdown GT1-7 cells could return the levels of p62 and ubiquitinated proteins expression to normal. Moreover, the efficiency of autophagosome/lysosome fusion and lysosomal clearance in WT compared to *Magel2*-knockdown GT1-7 cells can be examined using LysoTracker staining (Lee *et al.*, 2010) or double-immunofluorescence labelling LC3 and lysosome-associated membrane protein type 1 (LAMP-1) or LAMP-2, which are markers of lysosomes (Raben *et al.*, 2009).

I also discovered that Magel2 is connected to muscle function. Loss of Magel2 results in reduced muscle mass and is accompanied by changes in the fiber size distribution (Figure *3.12* and Figure *3.14*). The changes in the fiber size distribution might be related to increase or decrease in specific fiber type and these changes could be determined by using antibodies against specific fiber types (BA-D5 antibody for MHCI, SC-71 antibody for MHCIIA, 6H1 antibody for MHCIID/X, and BF-F3 antibody for MHCIIB) and visualized by immunohistochemistry. In addition, experiments that had been done looking at muscle histology can be repeated using mice at younger ages to elucidate whether changes in fiber size are congenital or progressive. I also proposed a

possible role of Magel2 in myogenic differentiation and regeneration. *In vitro* experiments using primary myoblasts isolated from WT and *Magel2*-null mice can be performed to investigate how Magel2 exerts its effect on myogenesis. It is anticipated this project will be a steppingstone to better understand the role of Magel2 in regulating autophagy and muscle function, as well as to identify a therapeutic target that can improve obesity and musculoskeletal abnormalities in PWS and Schaaf-Yang Syndrome.

References

Aebischer, J., Sturny, R., Andrieu, D., Rieusset, A., Schaller, F., Geib, S., Raoul, C., and Muscatelli, F. (2011). Necdin protects embryonic motoneurons from programmed cell death. PLoS One *6*, e23764.

Ao, X., Zou, L., and Wu, Y. (2014). Regulation of autophagy by the Rab GTPase network. Cell Death Differ. *21*, 348–358.

Ap, A. *et al.* (2013). Central precocious puberty caused by mutations in the imprinted gene MKRN3. N. Engl. J. Med. *368*.

Augusto, V., Padovani, C. R., Eduardo, G., and Campos, R. (2004). Skeletal Muscle Fiber Types in C57Bl6J Mice. Brazilian J. Morphol. Sci. *21*, 89–94.

Barker, P. a, and Salehi, A. (2002). The MAGE proteins: emerging roles in cell cycle progression, apoptosis, and neurogenetic disease. J. Neurosci. Res. *67*, 705–712.

Bekx, M. T., Carrel, A. L., Shriver, T. C., Li, Z., and Allen, D. B. (2003). Decreased energy expenditure is caused by abnormal body composition in infants with Prader-Willi Syndrome. J. Pediatr. *143*, 372–376.

Bischof, J. M., Stewart, C. L., and Wevrick, R. (2007). Inactivation of the mouse Magel2 gene results in growth abnormalities similar to Prader-Willi syndrome. Hum. Mol. Genet. *16*, 2713–2719.

Bjørkøy, G., Lamark, T., Brech, A., Outzen, H., Perander, M., Overvatn, A., Stenmark, H., and Johansen, T. (2005). p62/SQSTM1 forms protein aggregates degraded by autophagy and has a protective effect on huntingtin-induced cell death. J. Cell Biol. *171*, 603–614.

Boccaccio, I., Glatt-Deeley, H., Watrin, F., Roeckel, N., Lalande, M., and Muscatelli, F. (1999). The Human Magel2 Gene and Its Mouse Homologue Are Paternally Expressed and Mapped to the Prader-Willi Region. Hum. Mol. Genet. *8*, 2497–2505.

Bodine, S. C. *et al.* (2001). Identification of ubiquitin ligases required for skeletal muscle atrophy. Science *294*, 1704–1708.

Bodine, S. C., and Baehr, L. M. (2014). Skeletal muscle atrophy and the E3 ubiquitin ligases MuRF1 and MAFbx/atrogin-1. Am. J. Physiol. Endocrinol. Metab. *307*, E469–E484.

Boland, B., Kumar, A., Lee, S., Platt, F. M., Wegiel, J., Yu, W. H., and Nixon, R. A. (2008). Autophagy Induction and Autophagosome Clearance in Neurons: Relationship to Autophagic Pathology in Alzheimer's Disease. J. Neurosci. *28*, 6926–6937.

Bonaldo, P., and Sandri, M. (2013). Cellular and molecular mechanisms of muscle atrophy. Dis. Model. Mech. *6*, 25–39.

Brunner, D., Appl, H., Pfaller, W., and Gstraunthaler, G. (2010). Serum-free Cell Culture : The Serum-free Media Interactive Online Database. Altern. to Anim. Exp. *27*, 53–62.

Bush, J. R., and Wevrick, R. (2008). The Prader–Willi syndrome protein necdin interacts with the E1A-like inhibitor of differentiation EID-1 and promotes myoblast differentiation. Differentiation *76*, 994–1005.

Bush, J. R., and Wevrick, R. (2010). Loss of Necdin impairs myosin activation and delays cell polarization. Genesis *48*, 540–553.

Butler, J. V, Whittington, J. E., Holland, A. J., Boer, H., Clarke, D., and Webb, T. (2002). Prevalence of, and risk factors for, physical ill-health in people with Prader-Willi syndrome: A population-based study. Dev. Med. Child Neurol. *44*, 248–255.

Butler, M. G., Theodoro, M. F., Bittel, D. C., and Donnelly, J. E. (2007). Energy expenditure and physical activity in Prader-Willi syndrome: comparison with obese subjects. Am. J. Med. Genet. A *143A*, 449–459.

Capodaglio, P., Menegoni, F., Vismara, L., Cimolin, V., Grugni, G., and Galli, M. (2011). Characterisation of balance capacity in Prader-Willi patients. Res. Dev. Disabil. *32*, 81–86.

Capodaglio, P., Vismara, L., Menegoni, F., Baccalaro, G., Galli, M., and Grugni, G. (2009). Strength characterization of knee flexor and extensor muscles in Prader-Willi and obese patients. BMC Musculoskelet. Disord. *10*, 47.

Carrel, A. L., Myers, S. E., Whitman, B. Y., Eickhoff, J., and Allen, D. B. (2010). Long-term growth hormone therapy changes the natural history of body composition and motor function in children with prader-willi syndrome. J. Clin. Endocrinol. Metab. *95*, 1131–1136.

Cassidy, S. B., Schwartz, S., Miller, J. L., and Driscoll, D. J. (2012). Prader-Willi syndrome. Genet. Med. *14*.

Cavaillé, J., Buiting, K., Kiefmann, M., Lalande, M., Brannan, C. I., Horsthemke, B., Bachellerie, J. P., Brosius, J., and Hüttenhofer, A. (2000). Identification of brain-specific and imprinted small nucleolar RNA genes exhibiting an unusual genomic organization. Proc. Natl. Acad. Sci. U. S. A. *97*, 14311–14316.

Chomez, P., De Backer, O., Bertrand, M., De Plaen, E., Boon, T., and Lucas, S. (2001). An Overview of the MAGE Gene Family with the Identification of All Human Members of the Family. Cancer Res. *61*, 5544–5551.

Clarke, B. A. *et al.* (2007). The E3 Ligase MuRF1 degrades myosin heavy chain protein in dexamethasone-treated skeletal muscle. Cell Metab. *6*, 376–385.

Coupe, B., and Bouret, S. G. (2013). Development of the hypothalamic melanocortin system. Front. Endocrinol. (Lausanne). *4*, 38.

Coupé, B., Ishii, Y., Dietrich, M. O., Komatsu, M., Horvath, T. L., and Bouret, S. G. (2012). Loss of autophagy in pro-opiomelanocortin neurons perturbs axon growth and causes metabolic dysregulation. Cell Metab. *15*, 247–255.

Dayalu, P., and Albin, R. L. (2015). Huntington Disease: Pathogenesis and Treatment. Neurol. Clin. *33*, 101–114.

Deponti, D. *et al.* (2007). Necdin mediates skeletal muscle regeneration by promoting myoblast survival and differentiation. J. Cell Biol. *179*, 305–319.

Devos, J., Weselake, S. V, and Wevrick, R. (2011). Magel2, a Prader-Willi syndrome candidate gene, modulates the activities of circadian rhythm proteins in cultured cells. J. Circadian Rhythms *9*, 12.

Doyle, J. M., Gao, J., Wang, J., Yang, M., and Potts, P. R. (2010). MAGE-RING protein complexes comprise a family of E3 ubiquitin ligases. Mol. Cell *39*, 963–974.

Edouard, T., Deal, C., Van Vliet, G., Gaulin, N., Moreau, A., Rauch, F., and Alos, N. (2012). Muscle-Bone Characteristics in Children with Prader-Willi Syndrome. J. Clin. Endocrinol. Metab. *97*, E275–E281.

Eiholzer, U., l'Allemand, D., Rousson, V., Schlumpf, M., Gasser, T., Girard, J., Grüters, A., and Simoni, M. (2006). Hypothalamic and gonadal components of hypogonadism in boys with Prader-Labhart- Willi syndrome. J. Clin. Endocrinol. Metab. *91*, 892–898.

Eiholzer, U., L'allemand, D., Schlumpf, M., Rousson, V., Gasser, T., and Fusch, C. (2004). Growth hormone and body composition in children younger than 2 years with Prader-Willi syndrome. J. Pediatr. *144*, 753–758.

Eiholzer, U., Nordmann, Y., l'Allemand, D., Schlumpf, M., Schmid, S., and Kromeyer-Hauschild, K. (2003). Improving body composition and physical activity in Prader-Willi Syndrome. J. Pediatr. *142*, 73–78.

Eldar-Geva, T., Hirsch, H. J., Benarroch, F., Rubinstein, O., and Gross-Tsur, V. (2010). Hypogonadism in females with Prader-Willi syndrome from infancy to adulthood: Variable combinations of a primary gonadal defect and hypothalamic dysfunction. Eur. J. Endocrinol. *162*, 377–384.

Elmquist, J. K., Coppari, R., Balthasar, N., Ichinose, M., and Lowell, B. B. (2005). Identifying hypothalamic pathways controlling food intake, body weight, and glucose homeostasis. J. Comp. Neurol. *493*, 63–71.

Fleming, A., Noda, T., Yoshimori, T., and Rubinsztein, D. C. (2011). Chemical modulators of autophagy as biological probes and potential therapeutics. Nat. Chem. Biol. *7*, 9–17.

Frayn, K. N., and Maycock, P. F. (1979). Regulation of protein metabolism by a physiological

concentration of insulin in mouse soleus and extensor digitorum longus muscles. Effects of starvation and scald injury. Biochem. J. *184*, 323–330.

Gérard, M., Hernandez, L., Wevrick, R., and Stewart, C. L. (1999). Disruption of the mouse necdin gene results in early post-natal lethality. Nat. Genet. *23*, 199–202.

Glenn, C. C., Driscoll, D. J., Yang, T. P., and Nicholls, R. D. (1997). Genomic imprinting: potential function and mechanisms revealed by the Prader-Willi and Angelman syndromes. Mol. Hum. Reprod. *3*, 321–332.

Glenn, C. C., Saitoh, S., Jong, M. T., Filbrandt, M. M., Surti, U., Driscoll, D. J., and Nicholls, R. D. (1996). Gene structure, DNA methylation, and imprinted expression of the human SNRPN gene. Am. J. Hum. Genet. *58*, 335–346.

Glick, D., Barth, S., and Macleod, K. F. (2010). Autophagy : cellular and molecular mechanisms. J. Pathol. *221*, 3–12.

Goldberg, A. L. (2012). Development of proteasome inhibitors as research tools and cancer drugs. J. Cell Biol. *199*, 583–588.

Goldstone, A. P., Brynes, A. E., Thomas, E. L., Bell, J. D., Frost, G., Holland, A., Ghatei, M. A., and Bloom, S. R. (2002). Resting metabolic rate, plasma leptin concentrations, leptin receptor expression, and adipose tissue measured by whole-body magnetic resonance imaging in women with Prader-Willi syndrome. Am J Clin Nutr *75*, 468–475.

Gray, T. a, Saitoh, S., and Nicholls, R. D. (1999). An imprinted, mammalian bicistronic transcript encodes two independent proteins. Proc. Natl. Acad. Sci. U. S. A. *96*, 5616–5621.

Grumati, P. *et al.* (2010). Autophagy is defective in collagen VI muscular dystrophies, and its reactivation rescues myofiber degeneration. Nat. Med. *16*, 1313–1320.

Gunay-aygun, M., Schwartz, S., Heeger, S., Riordan, M. A. O., Cassidy, S. B., Background, A., and Pws, P. (2001). Criteria and Proposed Revised Criteria. Pediatrics *108*, 1–5.

Hamzi, K., Itto, A. Ben, Nassereddine, S., and Nadifi, S. (2010). Prader-Willi syndrome: Methylation study or fluorescence in situ hybridization first? Indian J. Hum. Genet. *16*, 172–174.

Hao, Y.-H., Doyle, J. M., Ramanathan, S., Gomez, T. S., Jia, D., Xu, M., Chen, Z. J., Billadeau, D. D., Rosen, M. K., and Potts, P. R. (2013). Regulation of WASH-dependent actin polymerization and protein trafficking by ubiquitination. Cell *152*, 1051–1064.

Hara, T. *et al.* (2006). Suppression of basal autophagy in neural cells causes neurodegenerative disease in mice. Nature *441*, 885–889.

Harada, H. *et al.* (2013). Deficiency of p62/Sequestosome 1 causes hyperphagia due to leptin resistance in the brain. J. Neurosci. *33*, 14767–14777.

Hasegawa, K., and Yoshikawa, K. (2008). Necdin regulates p53 acetylation via Sirtuin1 to modulate DNA damage response in cortical neurons. J. Neurosci. *28*, 8772–8784.

Hayashi, Y., Matsuyama, K., Takagi, K., Sugiura, H., and Yoshikawa, K. (1995). Arrest of cell growth by necdin, a nuclear protein expressed in postmitotic neurons. Biochem. Biophys. Res. Commun. *213*, 317–324.

Holm, V. a, Cassidy, S. B., Butler, M. G., Hanchett, J. M., Greenswag, L. R., Whitman, B. Y., and Greenberg, F. (1993). Prader-Willi syndrome: consensus diagnostic criteria. Pediatrics *91*, 398–402.

Huang, Z., Fujiwara, K., Minamide, R., Hasegawa, K., and Yoshikawa, K. (2013). Necdin controls proliferation and apoptosis of embryonic neural stem cells in an oxygen tension-dependent manner. J. Neurosci. *33*, 10362–10373.

Jankovic, J. (2008). Parkinson's disease: clinical features and diagnosis. J. Neurol. Neurosurg. Psychiatry *79*, 368–376.

Jong, M. T., Gray, T. A., Ji, Y., Glenn, C. C., Saitoh, S., Driscoll, D. J., and Nicholls, R. D. (1999). A novel imprinted gene, encoding a RING zinc-finger protein, and overlapping antisense transcript in the Prader-Willi syndrome critical region. Hum. Mol. Genet. *8*, 783–793.

Kadi, F. (2008). Cellular and molecular mechanisms responsible for the action of testosterone on human skeletal muscle. A basis for illegal performance enhancement. Br. J. Pharmacol. *154*, 522–528.

Kaushik, S., Arias, E., Kwon, H., Lopez, N. M., Athonvarangkul, D., Sahu, S., Schwartz, G. J., Pessin, J. E., and Singh, R. (2012). Loss of autophagy in hypothalamic POMC neurons impairs lipolysis. EMBO Rep. *13*, 258–265.

Kaushik, S., Rodriguez-Navarro, J. A., Arias, E., Kiffin, R., Sahu, S., Schwartz, G. J., Cuervo, A. M., and Singh, R. (2011). Autophagy in hypothalamic AgRP neurons regulates food intake and energy balance. Cell Metab. *14*, 173–183.

Kemp, J. G., Blazev, R., Stephenson, D. G., and Stephenson, G. M. M. (2009). Morphological and biochemical alterations of skeletal muscles from the genetically obese (ob/ob) mouse. Int. J. Obes. (Lond). *33*, 831–841.

Kiriyama, Y., and Nochi, H. (2015). The Function of Autophagy in Neurodegenerative Diseases. Int. J. Mol. Sci. *16*, 26797–26812.

Kirkin, V. *et al.* (2009). A Role for NBR1 in Autophagosomal Degradation of Ubiquitinated Substrates. Mol. Cell *33*, 505–516.

Kishore, S., and Stamm, S. (2006). Regulation of Alternative Splicing by snoRNAs Regulation of Alternative Splicing by snoRNAs. Cold Spring Harb. Lab. Press *LXXI*, 329–334.

Kobayashi, M., Taniura, H., and Yoshikawa, K. (2002). Ectopic expression of necdin induces differentiation of mouse neuroblastoma cells. J. Biol. Chem. *277*, 42128–42135.

Komatsu, M. *et al.* (2005). Impairment of starvation-induced and constitutive autophagy in Atg7-deficient mice. J. Cell Biol. *169*, 425–434.

Komatsu, M. *et al.* (2006). Loss of autophagy in the central nervous system causes neurodegeneration in mice. Nature *441*, 880–884.

Komatsu, M. *et al.* (2007a). Homeostatic Levels of p62 Control Cytoplasmic Inclusion Body Formation in Autophagy-Deficient Mice. Cell *131*, 1149–1163.

Komatsu, M., Wang, Q. J., Holstein, G. R., Friedrich, V. L., Iwata, J., Kominami, E., Chait, B. T., Tanaka, K., and Yue, Z. (2007b). Essential role for autophagy protein Atg7 in the maintenance of axonal homeostasis and the prevention of axonal degeneration. Proc. Natl. Acad. Sci. U. S. A. *104*, 14489–14494.

Kozlov, S. V, Bogenpohl, J. W., Howell, M. P., Wevrick, R., Panda, S., Hogenesch, J. B., Muglia, L. J., Van Gelder, R. N., Herzog, E. D., and Stewart, C. L. (2007). The imprinted gene Magel2 regulates normal circadian output. Nat. Genet. *39*, 1266–1272.

Kuma, A., Hatano, M., Matsui, M., Yamamoto, A., Nakaya, H., Yoshimori, T., Ohsumi, Y., Tokuhisa, T., and Mizushima, N. (2004). The role of autophagy during the early neonatal starvation period. Nature *432*, 1032–1036.

Laplante, M., and Sabatini, D. M. (2013). Regulation of mTORC1 and its impact on gene expression at a glance. J. Cell Sci. *126*, 1713–1719.

Ledbetter, D. H., Mascarello, J. T., Riccardi, V. M., Harper, V. D., Airhart, S. D., and Strobel, R. J. (1982). Chromosome 15 Abnormalities and the Prader-Willi Syndrome : A Follow-up Report of 40 Cases. Am. J. Hum. Genet. *34*, 278–285.

Lee, S. Walker, C L. Wevrick, R. (2003). Prader–Willi syndrome transcripts are expressed in phenotypically significant regions of the developing mouse brain. Gene Expr. Patterns *3*, 599–609.

Lee, J.-H. *et al.* (2010). Lysosomal proteolysis and autophagy require presenilin 1 and are disrupted by Alzheimer-related PS1 mutations. Cell *141*, 1146–1158.

Lee, M., Beggs, S. M., Gildea, D., Bupp, S., Lichtenberg, J., Trivedi, N. S., Comparative, N., Program, S., Hu, Y., and David, M. (2015). Necdin is a breast cancer metastasis suppressor that regulates the transcription of c-Myc. Oncotarget *6*, 31557–31568.

Lee, S., Kozlov, S., Hernandez, L., Chamberlain, S. J., Brannan, C. I., Stewart, C. L., and Wevrick, R. (2000). Expression and imprinting of MAGEL2 suggest a role in Prader-willi syndrome and the homologous murine imprinting phenotype. Hum. Mol. Genet. *9*, 1813–1819.

de Lind van Wijngaarden, R. F. A., de Klerk, L. W. L., Festen, D. A. M., and Hokken-Koelega, A. C. S. (2008). Scoliosis in Prader-Willi syndrome: prevalence, effects of age, gender, body mass index, lean body mass and genotype. Arch. Dis. Child. *93*, 1012–1016.

Livak, K. J., and Schmittgen, T. D. (2001). Analysis of relative gene expression data using real-time quantitative PCR and the 2(-Delta Delta C(T)) Method. Methods *25*, 402–408.
Mammucari, C. *et al.* (2007). FoxO3 controls autophagy in skeletal muscle in vivo. Cell Metab. *6*, 458–471.

Maruyama, K., Usami, M., Aizawa, T., and Yoshikawa, K. (1991). A novel brain-specific mRNA encoding nuclear protein (necdin) expressed in neurally differentiated embryonal carcinoma cells. Biochem. Biophys. Res. Commun. *178*, 291–296.

Masiero, E., Agatea, L., Mammucari, C., Blaauw, B., Loro, E., Komatsu, M., Metzger, D., Reggiani, C., Schiaffino, S., and Sandri, M. (2009). Autophagy is required to maintain muscle mass. Cell Metab. *10*, 507–515.

Masiero, E., and Sandri, M. (2010). Autophagy inhibition induces atrophy and myopathy in adult skeletal muscles. Autophagy *6*, 1–3.

Mejlachowicz, D., Nolent, F., Maluenda, J., Ranjatoelina-Randrianaivo, H., Giuliano, F., Gut, I., Sternberg, D., Laquerrière, A., and Melki, J. (2015). Truncating Mutations of MAGEL2, a Gene within the Prader-Willi Locus, Are Responsible for Severe Arthrogryposis. Am. J. Hum. Genet., 1–5.

Mercer, R. E., Michaelson, S. D., Chee, M. J. S., Atallah, T. A., Wevrick, R., and Colmers, W. F. (2013). Magel2 is required for leptin-mediated depolarization of POMC neurons in the hypothalamic arcuate nucleus in mice. PLoS Genet. *9*, e1003207.

Mercer, R. E., and Wevrick, R. (2009). Loss of magel2, a candidate gene for features of Prader-Willi syndrome, impairs reproductive function in mice. PLoS One *4*, e4291.

Miller, J. L., Lynn, C. H., Driscoll, D. C., Goldstone, A. P., Gold, J.-A., Kimonis, V., Dykens, E., Butler, M. G., Shuster, J. J., and Driscoll, D. J. (2011). Nutritional phases in Prader-Willi syndrome. Am. J. Med. Genet. A *155A*, 1040–1049.

Mizushima, N. (2010). The role of the Atg1/ULK1 complex in autophagy regulation. Curr. Opin. Cell Biol. *22*, 132–139.

Mizushima, N., Yamamoto, A., Matsui, M., Yoshimori, T., and Ohsumi, Y. (2004). In vivo analysis of autophagy in response to nutrient starvation using transgenic mice expressing a fluorescent autophagosome marker. Mol. Biol. Cell *15*, 1101–1111.

Nakamura, Y., Murakami, N., Iida, T., Asano, S., Ozeki, S., and Nagai, T. (2014a). Growth Hormone Treatment for Osteoporosis in Patients With Scoliosis of Prader-Willi syndrome. J. Orthop. Sci., 3–8.

Nakamura, Y., Murakami, N., Iida, T., Ozeki, S., Asano, S., Nohara, Y., and Nagai, T. (2014b). The characteristics of scoliosis in Prader-Willi syndrome (PWS): analysis of 58 scoliosis patients with PWS. J. Orthop. Sci., 17–22.

Neel, B. A., Lin, Y., and Pessin, J. E. (2013). Skeletal muscle autophagy: a new metabolic regulator. Trends Endocrinol. Metab. *24*, 635–643.

Nicholls, R. D., Knoll, J. H., Butler, M. G., Karam, S., and Lalande, M. (1989). Genetic imprinting suggested by maternal heterodisomy in nondeletion Prader-Willi syndrome. Nature *342*, 281–285.

Nixon, R. A. (2013). The role of autophagy in neurodegenerative disease. Nat. Med. *19*, 983–997.

Nixon, R. A., Wegiel, J., Kumar, A., Yu, W. H., Peterhoff, C., Cataldo, A., and Cuervo, A. M. (2005). Extensive Involvement of Autophagy in Alzheimer Disease: An Immuno-Electron Microscopy Study. J. Neuropathol. Exp. Neurol. *64*, 113–122.

Oberbach, A., Bossenz, Y., Lehmann, S., Niebauer, J., Adams, V., Paschke, R., Schön, M. R., Blüher, M., and Punkt, K. (2006). Altered fiber distribution and fiber-specific glycolytic and oxidative enzyme activity in skeletal muscle of patients with type 2 diabetes. Diabetes Care *29*, 895–900.

Ozçelik, T., Leff, S., Robinson, W., Donlon, T., Lalande, M., Sanjines, E., Schinzel, A., and Francke, U. (1992). Small nuclear ribonucleoprotein polypeptide N (SNRPN), an expressed gene in the Prader-Willi syndrome critical region. Nat. Genet. *2*, 265–269.

Pellegrinelli, V., Rouault, C., Rodriguez-Cuenca, S., Albert, V., Edom-Vovard, F., Vidal-Puig, A., Clément, K., Butler-Browne, G. S., and Lacasa, D. (2015). Human Adipocytes Induce Inflammation and Atrophy in Muscle Cells During Obesity. Diabetes *64*, 3121–3134.

Pessina, P., Conti, V., Tonlorenzi, R., Touvier, T., Meneveri, R., Cossu, G., and Brunelli, S. (2012). Necdin enhances muscle reconstitution of dystrophic muscle by vessel-associated progenitors, by promoting cell survival and myogenic differentiation. Cell Death Differ. *19*, 827–838.

Pravdivyi, I., Ballanyi, K., Colmers, W. F., and Wevrick, R. (2015). Progressive postnatal decline in leptin sensitivity of arcuate hypothalamic neurons in the Magel2-null mouse model of Prader-Willi syndrome. Hum. Mol. Genet. *24*, 4276–4283.

Quan, W. *et al.* (2012). Role of hypothalamic proopiomelanocortin neuron autophagy in the control of appetite and leptin response. Endocrinology *153*, 1817–1826.

Raben, N., Shea, L., Hill, V., and Plotz, P. (2009). Monitoring autophagy in lysosomal storage disorders. Methods Enzymol. *453*, 417–449.

Ravikumar, B. *et al.* (2004). Inhibition of mTOR induces autophagy and reduces toxicity of polyglutamine expansions in fly and mouse models of Huntington disease. Nat. Genet. *36*, 585–

595.

Reus, L., van Vlimmeren, L. a, Staal, J. B., Janssen, A. J. W. M., Otten, B. J., Pelzer, B. J., and Nijhuis-van der Sanden, M. W. G. (2013). Objective evaluation of muscle strength in infants with hypotonia and muscle weakness. Res. Dev. Disabil. *34*, 1160–1169.

Reus, L., Zwarts, M., van Vlimmeren, L. A., Willemsen, M. A., Otten, B. J., and Nijhuis-van der Sanden, M. W. G. (2011). Motor problems in Prader–Willi syndrome: A systematic review on body composition and neuromuscular functioning. Neurosci. Biobehav. Rev. *35*, 956–969.

Robinson, W. P., Bottani, a, Xie, Y. G., Balakrishman, J., Binkert, F., Mächler, M., Prader, a, and Schinzel, a (1991). Molecular, cytogenetic, and clinical investigations of Prader-Willi syndrome patients. Am. J. Hum. Genet. *49*, 1219–1234.

Rui, Y.-N. *et al.* (2015). Huntingtin functions as a scaffold for selective macroautophagy. Nat. Cell Biol. *17*, 262–275.

Runte, M., Hüttenhofer, A., Groß, S., Kiefmann, M., Horsthemke, B., and Buiting, K. (2001). The IC-SNURF–SNRPN transcript serves as a host for multiple small nucleolar RNA species and as an antisense RNA for UBE3A. Hum. Mol. Genet. *10*, 2687–2700.

Rusten, T. E., and Stenmark, H. (2009). How do ESCRT proteins control autophagy? J. Cell Sci. *122*, 2179–2183.

Saito, T., Nakamura, A., Aoki, Y., Yokota, T., Okada, T., Osawa, M., and Takeda, S. (2010). Antisense PMO found in dystrophic dog model was effective in cells from exon 7-deleted DMD patient. PLoS One *5*, e12239.

Sanchez, A. M. J., Bernardi, H., Py, G., and Candau, R. B. (2014). Autophagy is essential to support skeletal muscle plasticity in response to endurance exercise. Am. J. Physiol. Regul. Integr. Comp. Physiol. *307*, R956–R969.

Sandri, M. (2008). Signaling in muscle atrophy and hypertrophy. Physiology (Bethesda). *23*, 160–170.

Schaaf, C. P. *et al.* (2013). Truncating mutations of MAGEL2 cause Prader-Willi phenotypes and autism. Nat. Genet. *45*, 1405–1408.

Schaller, F., Watrin, F., Sturny, R., Massacrier, A., Szepetowski, P., and Muscatelli, F. (2010). A single postnatal injection of oxytocin rescues the lethal feeding behaviour in mouse newborns deficient for the imprinted Magel2 gene. Hum. Mol. Genet. *19*, 4895–4905.

Schiaffino, S., and Reggiani, C. (1994). Myosin isoforms in mammalian skeletal muscle. J Appl Physiol *77*, 493–501.

Schoeller, D. a., Levitsky, L. L., Bandini, L. G., Dietz, W. W., and Walczak, a. (1988). Energy

expenditure and body composition in Prader-Willi syndrome. Metabolism *37*, 115–120.
Scott, M. S., and Ono, M. (2011). From snoRNA to miRNA: Dual function regulatory non-coding RNAs. Biochimie *93*, 1987–1992.

Serra, C., Tangherlini, F., Rudy, S., Lee, D., Toraldo, G., Sandor, N. L., Zhang, A., Jasuja, R., and Bhasin, S. (2013). Testosterone improves the regeneration of old and young mouse skeletal muscle. J. Gerontol. A. Biol. Sci. Med. Sci. *68*, 17–26.

Shaffer, L. G., Agan, N., Goldberg, J. D., Ledbetter, D. H., Longshore, J. W., and Cassidy, S. B. (2001). American College of Medical Genetics statement on diagnostic testing for uniparental disomy. Genet. Med. *3*, 206–211.

Shang, L., and Wang, X. (2011). AMPK and mTOR coordinate the regulation of Ulk1 and mammalian autophagy initiation. Autophagy *7*, 924–926.

Shibata, M., Lu, T., Furuya, T., Degterev, A., Mizushima, N., Yoshimori, T., MacDonald, M., Yankner, B., and Yuan, J. (2006). Regulation of intracellular accumulation of mutant Huntingtin by Beclin 1. J. Biol. Chem. *281*, 14474–14485.

Smith, A., Robson, L., Neumann, A., Mulcahy, M., Chabros, V., Deng, Z. M., Woodage, T., and Trent, R. J. (1993). Fluorescence in-situ hybridisation and molecular studies used in the characterisation of a Robertsonian translocation (13q15q) in Prader-Willi syndrome. Clin. Genet. *43*, 5–8.

Spitali, P., Grumati, P., Hiller, M., Chrisam, M., Aartsma-Rus, A., and Bonaldo, P. (2013). Autophagy is Impaired in the Tibialis Anterior of Dystrophin Null Mice. PLoS Curr. *5*, 1–12.

Steiger-Barraissoul, S., and Rami, A. (2009). Serum deprivation induced autophagy and predominantly an AIF-dependent apoptosis in hippocampal HT22 neurons. Apoptosis *14*, 1274–1288.

Stuart, C. a., McCurry, M. P., Marino, A., South, M. a., Howell, M. E. a, Layne, A. S., Ramsey, M. W., and Stone, M. H. (2013). Slow-twitch fiber proportion in skeletal muscle correlates with insulin responsiveness. J. Clin. Endocrinol. Metab. *98*, 2027–2036.

Sumathipala, D. S., Jayasekara, R. W., and Dissanayake, V. H. W. (2013). Clinical and genetic features of Huntington disease in Sri Lanka. BMC Neurol. *13*, 1–5.

Takazaki, R., Nishimura, I., and Yoshikawa, K. (2002). Necdin Is Required for Terminal Differentiation and Survival of Primary Dorsal Root Ganglion Neurons. Exp. Cell Res. *277*, 220–232.

Taniura, H., Matsumoto, K., and Yoshikawa, K. (1999). Physical and functional interactions of neuronal growth suppressor necdin with p53. J. Biol. Chem. *274*, 16242–16248.

Taniura, H., Taniguchi, N., Hara, M., and Yoshikawa, K. (1998). Necdin, a postmitotic neuron-

specific growth suppressor, interacts with viral transforming proteins and cellular transcription factor E2F1. J. Biol. Chem. *273*, 720–728.

Tennese, A. A., Gee, C. B., and Wevrick, R. (2008). Loss of the Prader-Willi syndrome protein necdin causes defective migration, axonal outgrowth, and survival of embryonic sympathetic neurons. Dev. Dyn. *237*, 1935–1943.

Torrado, M., Foncuberta, M. E., Perez, M. F. de C., Gravina, L. P., Araoz, H. V, Baialardo, E., and Chertkoff, L. P. (2013). Change in prevalence of congenital defects in children with Prader-Willi syndrome. Pediatrics *131*, e544–e549.

Whittington, J., Holland, A., Webb, T., Butler, J., Clarke, D., Boer, H., Centre, L. C., Warwickshire, N., Care, P., and Clinic, J. S. (2004). Academic underachievement by people with Prader – Willi syndrome. J. Intellect. Disabil. Res. *48*, 188–200.

Williams, K. W., and Elmquist, J. K. (2012). From neuroanatomy to behavior: central integration of peripheral signals regulating feeding behavior. Nat. Neurosci. *15*, 1350–1355.
Winslow, A. R. *et al.* (2010). α-Synuclein impairs macroautophagy: implications for Parkinson's disease. J. Cell Biol. *190*, 1023–1037.

Wolfgram, P. M., Carrel, A. L., and Allen, D. B. (2013). Long-term effects of recombinant human growth hormone therapy in children with Prader-Willi syndrome. Curr. Opin. Pediatr. *25*, 509–514.

Woodage, T., Deng, Z. M., Prasad, M., Smart, R., Lindeman, R., Christian, S. L., Ledbetter, D. H., Robson, L., Smith, A., and Trent, R. J. (1994). A variety of genetic mechanisms are associated with the Prader-Willi syndrome. Am. J. Med. Genet. *54*, 219–226.

Yamamoto, A., Tagawa, Y., Yoshimori, T., Moriyama, Y., Masaki, R., and Tashiro, Y. (1998). Bafilomycin A1 prevents maturation of autophagic vacuoles by inhibiting fusion between autophagosomes and lysosomes in rat hepatoma cell line, H-4-II-E cells. Cell Struct. Funct. *23*, 33–42.

Yu, W. H. *et al.* (2005). Macroautophagy--a novel Beta-amyloid peptide-generating pathway activated in Alzheimer's disease. J. Cell Biol. *171*, 87–98.

Zhao, J., Brault, J. J., Schild, A., Cao, P., Sandri, M., Schiaffino, S., Lecker, S. H., and Goldberg, A. L. (2007). FoxO3 coordinately activates protein degradation by the autophagic/lysosomal and proteasomal pathways in atrophying muscle cells. Cell Metab. *6*, 472–483.

Zheng, S., Clabough, E. B. D., Sarkar, S., Futter, M., Rubinsztein, D. C., and Zeitlin, S. O. (2010). Deletion of the huntingtin polyglutamine stretch enhances neuronal autophagy and longevity in mice. PLoS Genet. *6*, e1000838.